2-P

AMERICAN SCIENCE AND ENGINEERING

11 CARLETON STREET, CAMBRIDGE,
MASSACHUSETTS 02142 (617) 868-1600

30 MAY 1970

ASE-2438

FINAL REPORT FOR

HIGH RESOLUTION X-RAY IMAGES OF THE SUN USING A GRAZING INCIDENCE TELESCOPE FROM A SOLAR POINTING AEROBEE ROCKET

BY

J. DAVIS
A. DECAPRIO
R. HAGGERTY
A. KRIEGER
H. MANKO
W. REIDY
G. VAIANA
L. VANSPEYBROECK
T. ZEHNPFENNIG

JUN 1970
RECEIVED
NASA STI FACILITY
INPUT BRANCH

CONTRACT NO. NASW-1700

PREPARED FOR

NATIONAL AERONAUTICS
AND SPACE ADMINISTRATION
WASHINGTON, D. C. 20546

N70-29888
(ACCESSION NUMBER)
(THRU)
15
(PAGES)
1
(CODE)
CR-110356
(NASA CR OR TMX OR AD NUMBER)
14
(CATEGORY)

ASE-2438

FINAL REPORT FOR

CONTRACT NASW-1700

HIGH RESOLUTION X-RAY IMAGES OF THE SUN USING A GRAZING INCIDENCE TELESCOPE FROM A SOLAR POINTING AEROBEE ROCKET

Report Period April 1968 - March 1970

Prepared by

J. Davis, A. DeCaprio, R. Haggerty,
A. Krieger, H. Manko, W. Reidy, G. Vaiana,
L. VanSpeybroeck, T. Zehnpfennig

American Science & Engineering, Inc.
11 Carleton Street
Cambridge, Massachusetts 02142

Prepared for

National Aeronautics
and Space Administration
Washington, D. C. 20546

30 May 1970

Approved: H. Gursky, Vice President
Space Research Division

G. S. Vaiana, Head
Solar Physics Group

FOREWORD

This document is the final report of NASA Contract NASW-1700. The contract provided for the analysis of the flight film obtained under NASA Contract NASW-1555 (Aerobee 150, No. 4.209 flown on March 15, 1968) and for the refurbishment, calibration, testing, alignment and field support of a high resolution grazing incidence X-ray telescope system to be flown on an Aerobee 150 rocket (No. 4.263 flown on June 8, 1968) and further for the development of the film obtained on this flight. Because of a failure in the pointing control system of Aerobee 4.209 used in the first flight, the analysis has been limited to two exposures. During the second flight all systems operated correctly and the resulting X-ray images were of a higher resolution than any previously obtained. The flight also resulted in the high resolution observation of an X-ray flare.

The Project Scientist for this contract was Dr. Giuseppe S. Vaiana.

ACKNOWLEDGEMENTS

We gratefully acknowledge the dedicated support of the staffs of the Environmental Science Services Administration (ESSA), Sacramento Peak, McMath-Hulbert, Lockheed and Sagamore Hill observatories for providing flare alarm and ground measurements, and, in particular, Messrs. D. Buckman and R. Decker of ESSA for co-ordinating the alarm network. We are indebted to Drs. R. Howard and H. Zirin, Mt. Wilson and Palomar Observatories; Drs. W. Livingston and N. Sheeley, Kitt Peak National Observatory and Dr. W. Curtis, High Altitude Observatory, for providing us with additional ground based solar observations. We wish to thank the personnel of the Sounding Rocket Branch of NASA's Goddard Space Flight Center (GSFC), and in particular Mr. G.D. Patterson of the Pointing Systems Divisions, for their support prior to launch; and also the personnel of the Navy Ordinance Testing Facility, White Sands Missile Range (WSMR), for their support during the successful launch of 4.263 CS.

CONTENTS

		Page
1.0	INTRODUCTION	1-1
2.0	EXPERIMENTAL RESULTS	2-1
	2.1 Introduction	2-1
	2.2 Solar Morphology on March 15, 1968	2-3
	2.3 Solar X-ray Emission on March 15, 1968	2-6
	2.4 Aspect Information	2-10
	2.5 Energy Release of Active Regions	2-10
	2.6 Structure of the Flaring Region	2-16
	2.7 Solar X-ray Line Spectra	2-19
3.0	EXPERIMENTAL MODIFICATIONS, TESTING AND ALIGNMENT	3-1
	3.1 Experimental Hardware	3-1
	3.2 Repairs and Modifications	3-2
	3.3 Description of Tests	3-5
	Integration Tests	3-5
	Alignment of Eyes to Payload Optical Axis	3-5
	Vibration Testing	3-6
	Final Inspection	3-6
4.0	FLIGHT OF 4.263 CS	4-1
5.0	POST FLIGHT ANALYSIS AND RECOVERY	5-1
6.0	FLIGHT FILMS FROM 4.263 CS	6-1
7.0	CONCLUSIONS	7-1
APPENDIX A		
APPENDIX B		

ILLUSTRATIONS

Figure		Page
2.1	Exposure II: 2 seconds with a parylene filter and un-topcoated Pan-x film.	2-4
2.2	Exposure V: 2 seconds with a 1/2 mil Beryllium filter and un-topcoated Pan-x film.	2-5
2.3	Ground based ESSA solar activity maps.	2-7
2.4	Solar $H\alpha$ photograph taken March 15, 1968.	2-8
2.5	Angular displacement of the optical axis during Exposure I.	2-11
2.6	Angular displacement of the optical axis during Exposure II.	2-12
2.7	Two-dimensional isodensitometer tracing of Exposure II.	2-14
2.8	Integrals of the energy deposited on the film as a function of area for Exposure II.	2-15
2.9	Wavelength passbands of the telescope filter combinations.	2-17
2.10	One-dimensional isodensitometer scans of the flaring region visible on Exposure V.	2-18
6.1	Exposure 1: June 8, 1968	6-3
6.2	Exposure 2: June 8, 1968	6-4
6.3	Exposure 3: June 8, 1968	6-5
6.4	Exposure 4: June 8, 1968	6-6
6.5	Exposure 5: June 8, 1968	6-7
6.6	Exposure 6: June 8, 1968	6-8
6.7	Exposure 7: June 8, 1968	6-9
6.8	Exposure 8: June 8, 1968	6-10
6.9	Exposure 9: June 8, 1968	6-11
6.10	Exposure 10: June 8, 1968	6-12
6.11	Exposure 11: June 8, 1968	6-13
6.12	Exposure 12: June 8, 1968	6-14

TABLES

Table		Page
I	Exposure Sequence for March 15, 1968	2-2
II	Timing Sequence for June 8, 1968	3-3
III	Exposure Sequence for June 8, 1968	3-4

1.0 INTRODUCTION

AS&E has been involved in the development of X-ray imaging telescopes since 1960. The initial laboratory work was performed in the period 1960-1962 and demonstrated the feasibility of cylindrically symmetric double reflection optics of the type first proposed by Wolter for use in X-ray microscopy. The first application of devices of this type was to study the solar corona in a collaborative program with Dr. John Lindsay at NASA/GSFC. X-ray telescopes were flown on two solar pointing rockets, one in October 1963, and the second in March, 1965. This program resulted in the first solar X-ray images obtained with grazing incidence optics and clearly demonstrated the potential of this instrumental technique.

Satellite measurements are necessary to study long-term changes in the X-ray emission associated with active centers and the quiescent corona and to obtain a meaningful sample of X-ray flares. It was for this purpose that the AS&E X-ray spectroheliogram was flown on the OSO-IV satellite. This experiment has obtained continuous data for 2 1/2 years and is still operating.

As a result of these programs, the technology associated with grazing incidence optics advanced rapidly, and it became possible to obtain imaging systems with a resolution which was more than an order of magnitude better than that previously achieved. Arc-second resolution is desirable in studies of the solar corona, since it is reasonable to anticipate that the arc-second structure observed in the chromosphere may be reflected in the coronal X-ray distribution. In order to study this question and to study the fine structure associated with active center and flare emission, AS&E proposed a program of high resolution solar X-ray

studies using both broad band filter spectroscopy and the higher resolution ($\lambda/\Delta\lambda \approx 50$) transmission grating spectroscopy. This program consists of a series of rocket observations in the period from 1968 to 1971 to be followed by extended measurements in 1972 from the Apollo Telescope Mount.

The first rocket in this series, designated 4.209 CS, was launched on March 15, 1968. Subsequent flights have occurred on June 8, 1968, April 8 and November 4, 1969 and March 7, 1970. Analysis of the data obtained from these flights has produced the following major conclusions:

1). That much of the X-ray emission from the sun originates in the corona directly above active regions. These areas of the corona are characterized by higher local temperatures and increases in the particle density of at least an order of magnitude above the quiet corona.

2). That there exist within the emitting regions structures with dimensions of a few arc-seconds which often closely resemble the corresponding $H\alpha$ plage seen on the disc.

3). That the enhanced X-ray emission in the corona extends to considerable height (100,000 to 150,000 km) above its associated active region. The three-dimensional structure is generally complex and appears to be governed by the magnetic field which does <u>not</u> correspond to a simple bi-polar configuration within one active region.

4). That the spectra of flare regions are substantially harder than those of active regions. However significant differences are also present among the spectra of non-flaring active regions.

5). That there exist small, concentrated, point-like features which are associated with and correspond to bright

bi-polar chromospheric structures evident in the CaK spectro-heliograms.

The present contract (NASW-1700) provided for the analysis of the data obtained from the initial flight in the series (March 15, 1968) and support for the second flight of the rocket payload.

The statement of work for this contract is the following:

1. Reduce, analyze and prepare for publication the scientific data obtained from the solar X-ray experiment on the Aerobee rocket during performance of NASA contract NASW-1555. The data will consist of solar X-ray images. This analysis will include for the suitable exposures; (i) the introduction of aspect data on the film; (ii) microdensitometer tracing of the data; (iii) a conversion of photographic density into deposited energy values; (iv) an evaluation of fluxes for various significant features; and (v) the interpretation and publication of the findings.

2. Refurbish and calibrate a grazing incidence X-ray telescope system with an angular resolution of better than 10 arc-seconds to obtain solar X-ray photographs from an Aerobee rocket.

3. Refurbish one instrument housekeeping unit including commutators, timers and batteries; and instrument switching logic for use with the X-ray photographs from an Aerobee rocket.

4. Provide the necessary nose cone modifications, nose cone separation system, solar 'STRAP' sensor mounting, and instrument support structure for housing in an Aerobee rocket the items developed under 2 and 3 above.

5. Provide the necessary field support for integration and testing at GSFC of the assembled instrument with an Aerobee rocket.

6. Provide quality assurance by inspection and monitoring of fabrication of flight items fabricated hereunder.

7. Develop the instrument's flight film and submit a final report covering the effort performed on this contract.

The evaluation of the photographic data is presented in Section 2.0. The modifications to the instrument for the second flight are described in Section 3.0. Sections 4.0 and 5.0 are devoted to flight performance and post flight inspection respectively. The flight films of the second flight are presented in Section 6.0.

2.0 EXPERIMENTAL RESULTS

2.1 Introduction

The purpose of this experiment was to obtain high resolution spectroheliograms of the solar X-ray emission. The instrument consisted of a grazing incidence X-ray telescope, a 12 exposure camera, a transmission grating, and an electromechanical programmer. It has been described in detail in the final report for NASA Contract NASW-1555 (ASE-1953).

Because of the considerable interest in studying flare associated X-ray emission, the time of launch was chosen to coincide with a visible light flare. To facilitate this effort a direct telephone connection was established with ESSA and several observatories, and the rocket countdown was held at T-3 minutes. The rocket launch took place at 1904 UT March 15, 1968 immediately following the observation of a subflare.

The exposure sequence, the films and filters used in this experiment are listed in Table I. The first nine exposures were chosen to provide broad band X-ray spectroheliograms and one visible light image. For the last three exposures, a transmission grating with a resolving power of the order of 50 was positioned in the optical path to provide high resolution X-ray spectroheliograms.

In addition to the images obtained with the grazing incidence optics, two other images of the sun were placed on each film strip. The first was imaged with a 2 inch diameter achromatic doublet, the second with an 0.08 inch pinhole. The lens was designed to yield a high resolution (~2 seconds of arc) visible light picture which can be compared with ground based observa-

TABLE I

Exposure Sequence for Aerobee 4.209 Flown on March 15, 1968.

Exposure	Film	Filter	Transmission Grating	Exposure Time (seconds)
1	103-0	2 mil Beryllium	No	34
2	Pan x	Parylene c	No	2
3	Pan x	1/2 mil Beryllium	No	6
4	103-0	2 mil Beryllium	No	18
5	Pan x	1/2 mil Beryllium	No	2
6	103-0	1/2 mil Beryllium	No	6
7	103-0	1/2 mil Beryllium	No	18
8	Pan x	Neutral density for visible light image	No	2
9	103-0	Parylene c	No	6
10	103-0	1/2 mil Beryllium	Yes	5.5
11	103-0	Parylene	Yes	40
12	Ilford Commercial	1/2 mil Beryllium	Yes	35

All films except Ilford Commercial were untop-coated. The parylene filters are composed of 10,000 Å of parylene c coated with 5000 Å of aluminum.

tions to determine roll orientation. The pinhole image serves as an additional fiducial mark on the film which is required to determine the center of the solar disk in the X-ray image. Because of the failure of the attitude control system the images obtained were severly degraded. The failure resulted in the continuous oscillation of the optical axis over the solar disc with the subsequent smearing out of the features in the X-ray image. However during two of the short exposures (2 seconds) the oscillation of the rocket was slight and predominantly in one direction. Consequently the image degradation was moderate and the exposures are of scientific value. These X-ray exposures appear as Figures 2.1 and 2.2. At the bottom the original film strip negatives are reproduced.

2.2 Solar Morphology on March 15, 1968

On March 15, 1968 the sun was moderately active with a dozen calcium plages visible on the disc. These regions provided a good sample in age; two (McMath numbers 9265 and 9253) had been observed on at least the five previous solar rotations, while others were making their first appearances. It was one of the latter, McMath number 9267, which was responsible for the subflare at 1900 U.T. which was recorded during this experiment. This active region had been, since its first appearance on the east limb on March 12, one of the most prominent areas on the sun. While gradually increasing in sun spot area it was also the most impressive feature at 9.1 cm and by March 14 it had become the source of many small subflares. The frequency of subflares increased substantially on March 15 and it was shortly after the onset of one of these subflares that the rocket was launched. This particular subflare reached its maximum development at approximately 1903 U.T. and lasted about 10 minutes. Ground measurements of the photospheric magnetic field indicated

NOT REPRODUCIBLE

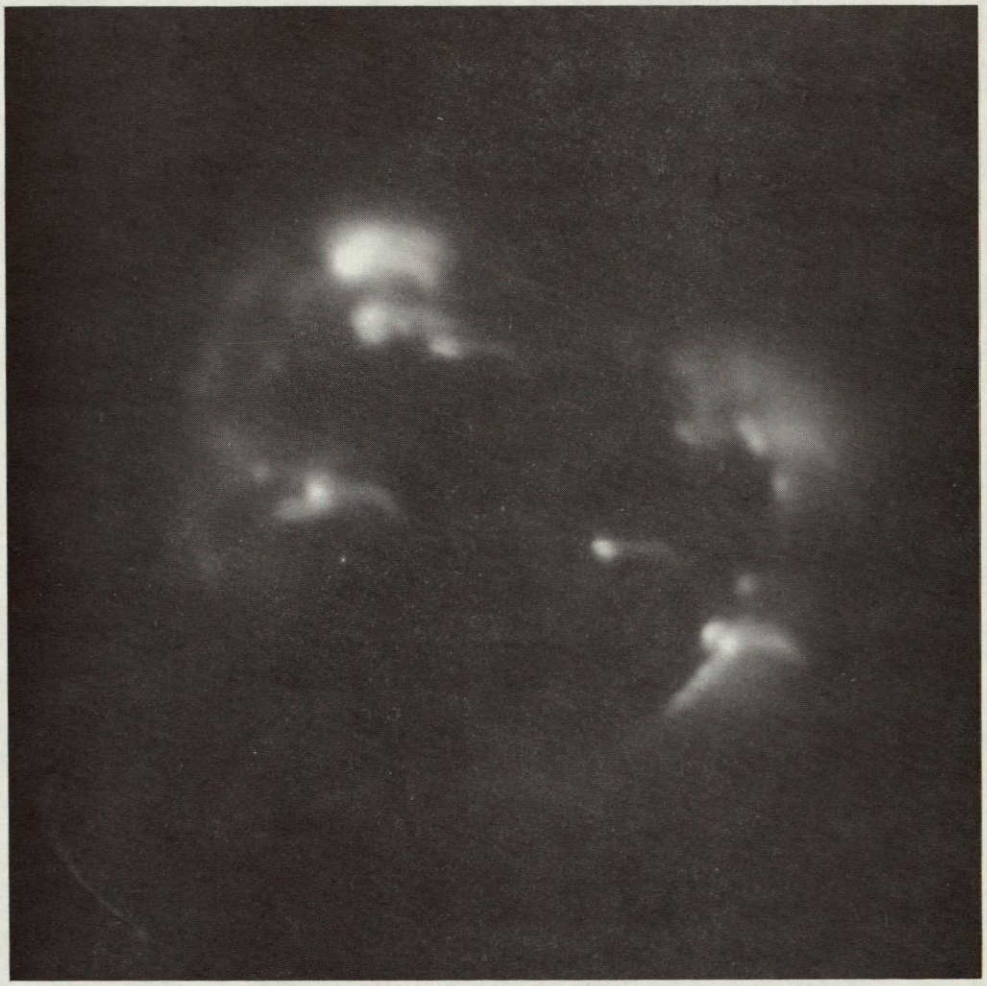

DZ-022

Figure 2.1 Exposure II: 2 seconds with a parylene filter and un-topcoated Pan-x film.

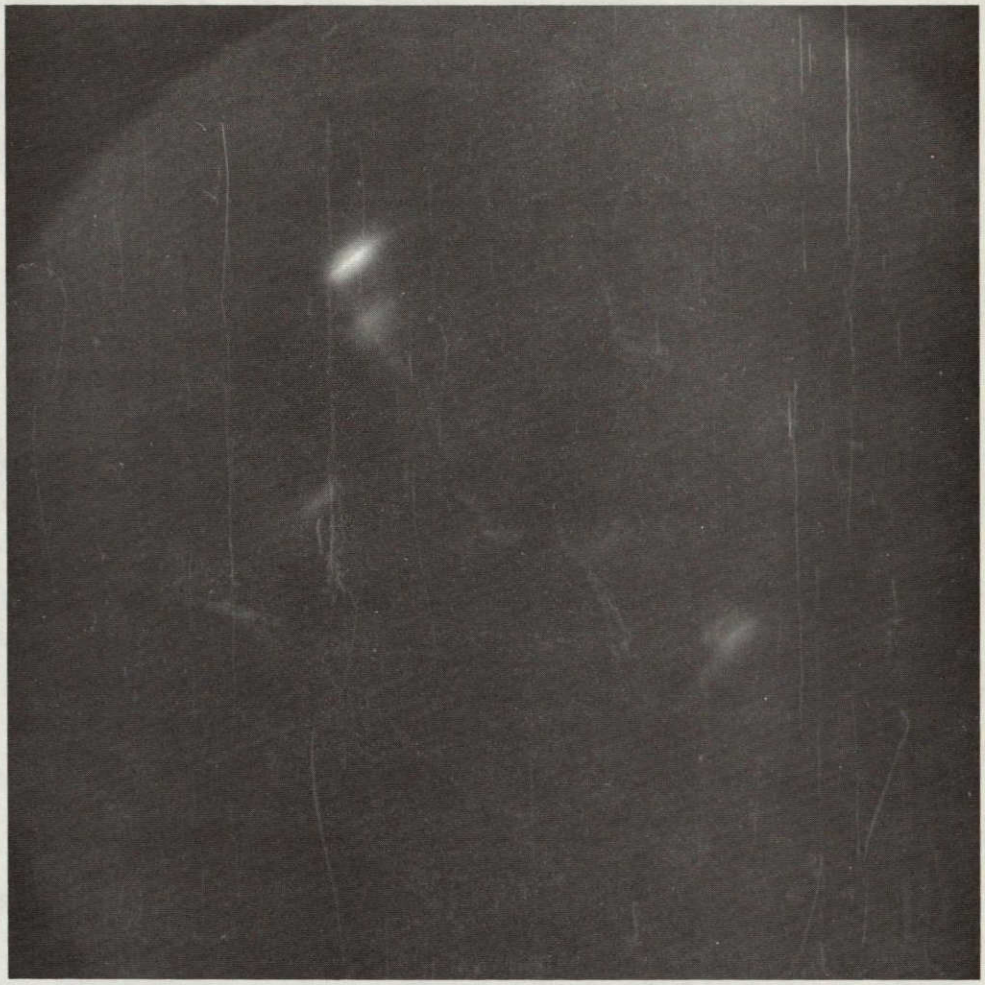

DZ-025

Figure 2.2 Exposure V: 2 seconds with a 1/2 mil Beryllium filter and un-topcoated Pan-x film.

that this region had a complex structure with very large field gradients in the vicinity of the flare. Maps of the solar activity on March 15, 1968, from ESSA Solar-Geophysical Data IER-FB-295 are shown in Figure 2. 3. Ground-based maps are shown for radio wavelengths (9. 1 and 21 cm), magnetic fields, and the CaK line.

2. 3 Solar X-Ray Emission on March 15, 1968

Inspection of the X-ray images shows that there are several regions on the sun which are emitting X-rays with wavelengths between 2 and 25 Å. The most impressive region is that associated directly with the flare. The 2 second exposure (Figure 2. 1) on un-topcoated Pan-x film taken with a parylene filter shows the flare somewhat overexposed in the northeast quadrant of the sun. The inner structure of the flare can be seen in the 2 second exposure taken with a 1/2 mil beryllium filter and un-topcoated Pan-x film (Figure 2. 2). Aspect information obtained from the visible light images indicates that the excursion of the optical axis produced by the faulty Attitude Control System (ACS) was predominantly in one direction during this exposure. Consequently if we examine the X-ray emission in a direction normal to the pointing excursion, we find that the flare has a hard core approximately 10 arc-seconds wide. We believe that this core region is directly associated with the region that produced the subflare at the time of launch.

All the active regions visible in Hα (Figure 2. 4) have counterparts in the X-ray photograph taken with the parylene filter. Even small Hα brightenings like those on the equator at 60° E and 60° W longitude have corresponding brightenings in X-rays. The activity at the southwest limb appears to be due to active centers which are behind the limb in Hα. The images also suggest a correlation between the localization of the X-ray emission and the age of active regions. In general, older regions

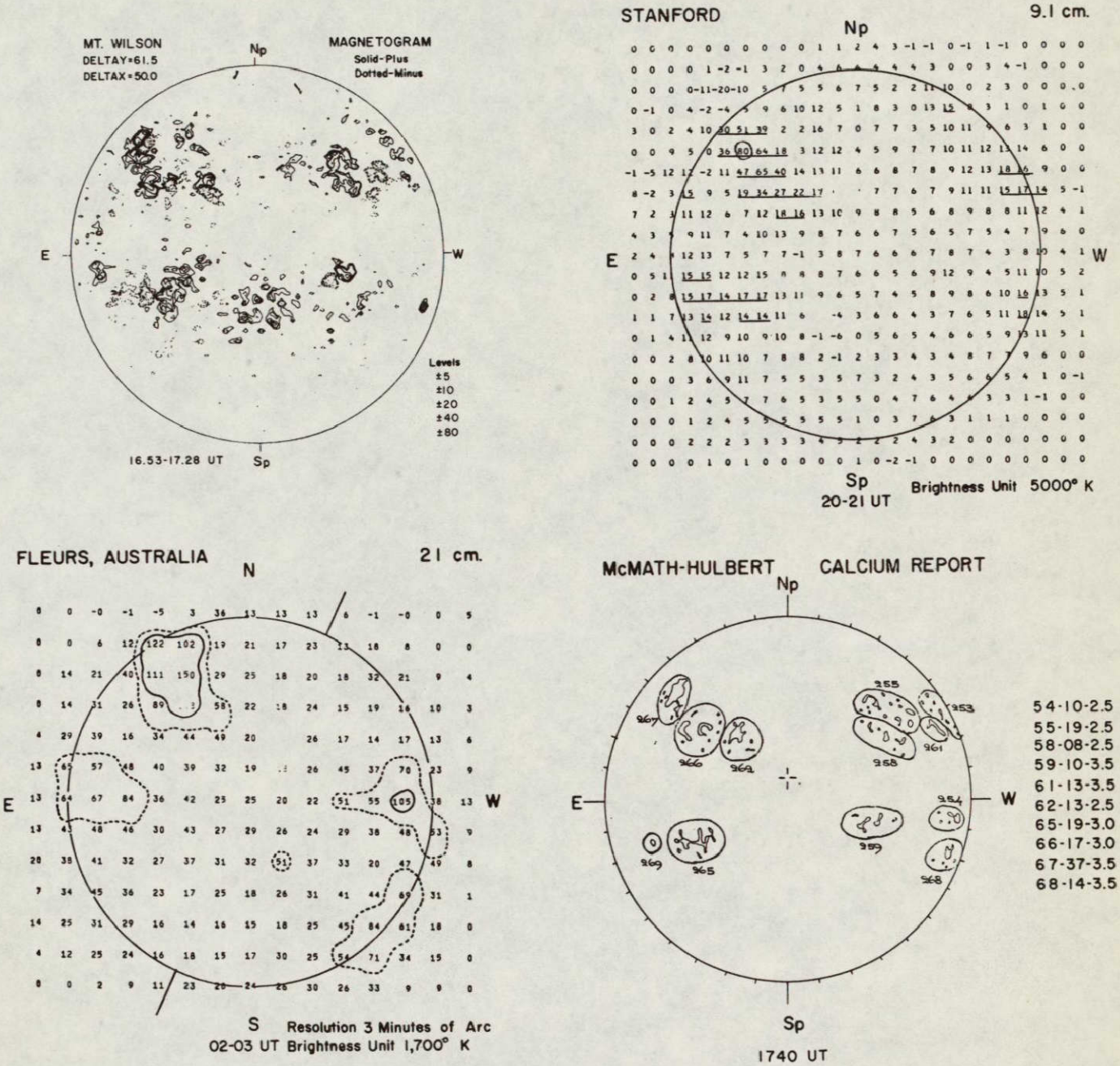

Figure 2.3 ESSA ground-based solar activity maps for March 15, 1968.

NOT REPRODUCIBLE

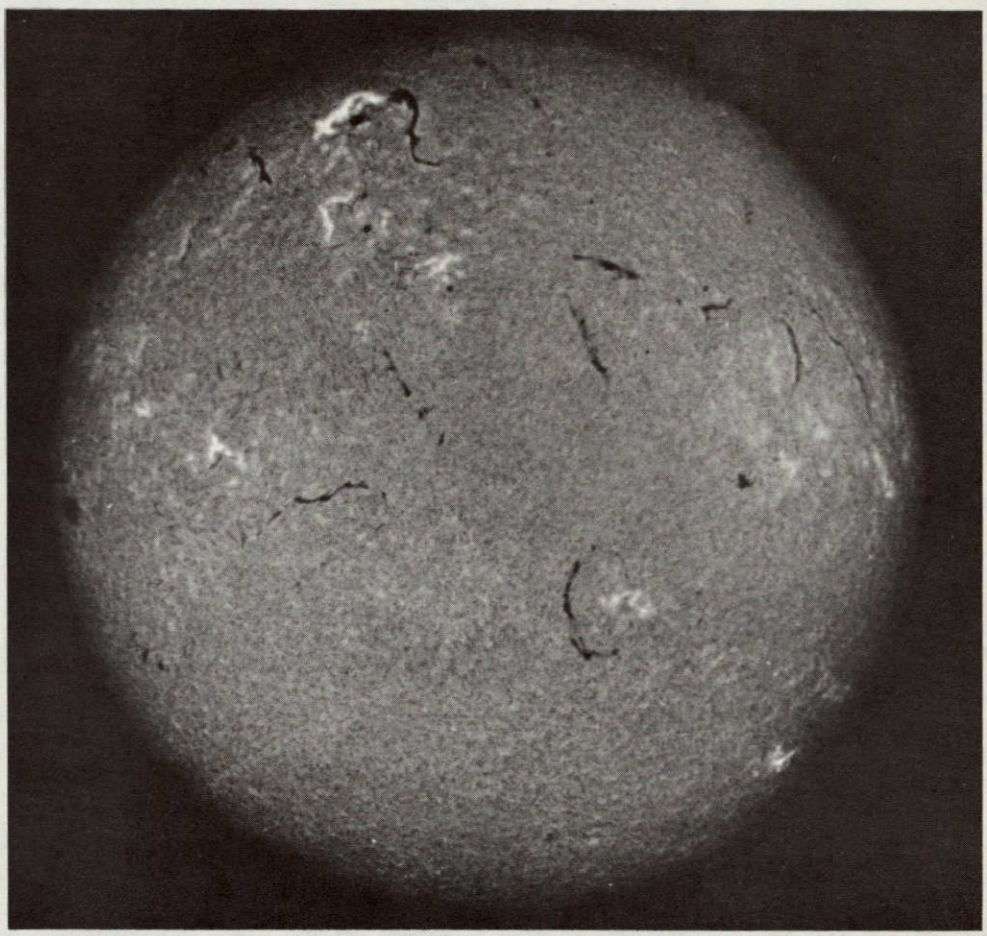

DZ-037

Figure 2.4 Solar H_α photograph taken March 15, 1968.

appear to have a more diffuse X-ray emission.

Closer examination reveals that correspondence between the Hα and X-ray images of a region depends upon its position on the solar disc. The X-ray emitting regions, when close to the center of the disc, appear to conform rather well with the shape and boundaries of the Hα bright regions. However the X-ray images near the limb show an extended structure which is not found in the Hα images. We are inclined to interpret these X-ray structures, which extend to heights of 100,000 km or more above the Hα plages, in terms of the loops which are observed in white light photographs of the corona.

The general coronal emission not associated with either flares or plages is also evident in the exposure, taken with the parylene filter, especially around the sun's southern pole. Since this emission appears to be absent in the longest exposure taken with the beryllium filter (18 seconds), we conclude, in agreement with conclusions from previous observations, that the general coronal emission is somewhat softer than the emission associated with the plages or the flare.

One of the main conclusions to be made from this analysis relates to the spatial correspondence between the X-ray and the Hα flare. This indicates a close link between the two emission phenomena. This is puzzling because of the large difference in degree of ionization required to produce the X-ray and the Hα radiation. One explanation is to consider a strong magnetic connection between the two regions. The X-ray emission associated with the other plage regions suggests such a magnetic link. However in the case of the flare the difficulty arises from having to assume a strong stable magnetic link while at the same time

having to require a sudden change in the magnetic field configuration to account for the energy released during the flare.

The overriding impression obtained from the photographs is that the X-ray emitting regions resemble the $H\alpha$ regions at the base of the corona, but that at higher levels the X-ray emitting regions are rich in looplike structures which interconnect $H\alpha$ active regions and are controlled by the solar magnetic field. This interpretation supports those theories that describe the additional heating in the upper layers of active regions in terms of an enhanced magnetic field.

2.4 Aspect Information

Aspect data, in terms of error signals proportional to the angular displacements of the pitch and yaw axes of the rocket referred to a co-ordinate system whose Z-axis is the vector direction to the center of the sun, are transmitted to the ground in real time throughout the flight. These data enable a reconstruction of the actual pointing direction of the X-ray telescope, with respect to the center of the sun, to be made for each exposure. Two of the resulting traces for exposures I and II are shown in Figures 2.5 and 2.6. It is obvious, by inspection, why no further analysis of exposure I was attempted and why the results produced by the analysis of exposure II are scientifically significant.

2.5 Energy Release of Active Regions

One of the important measurements which it is possible to make from the photographic images is the rate of energy release from the flare, individual active regions and the whole sun during the observation period. This measurement requires an integration of the photographic density distribution over the images of the various structures on the film and a knowledge of the energy response of the film and of the telescope-broadband filter combination.

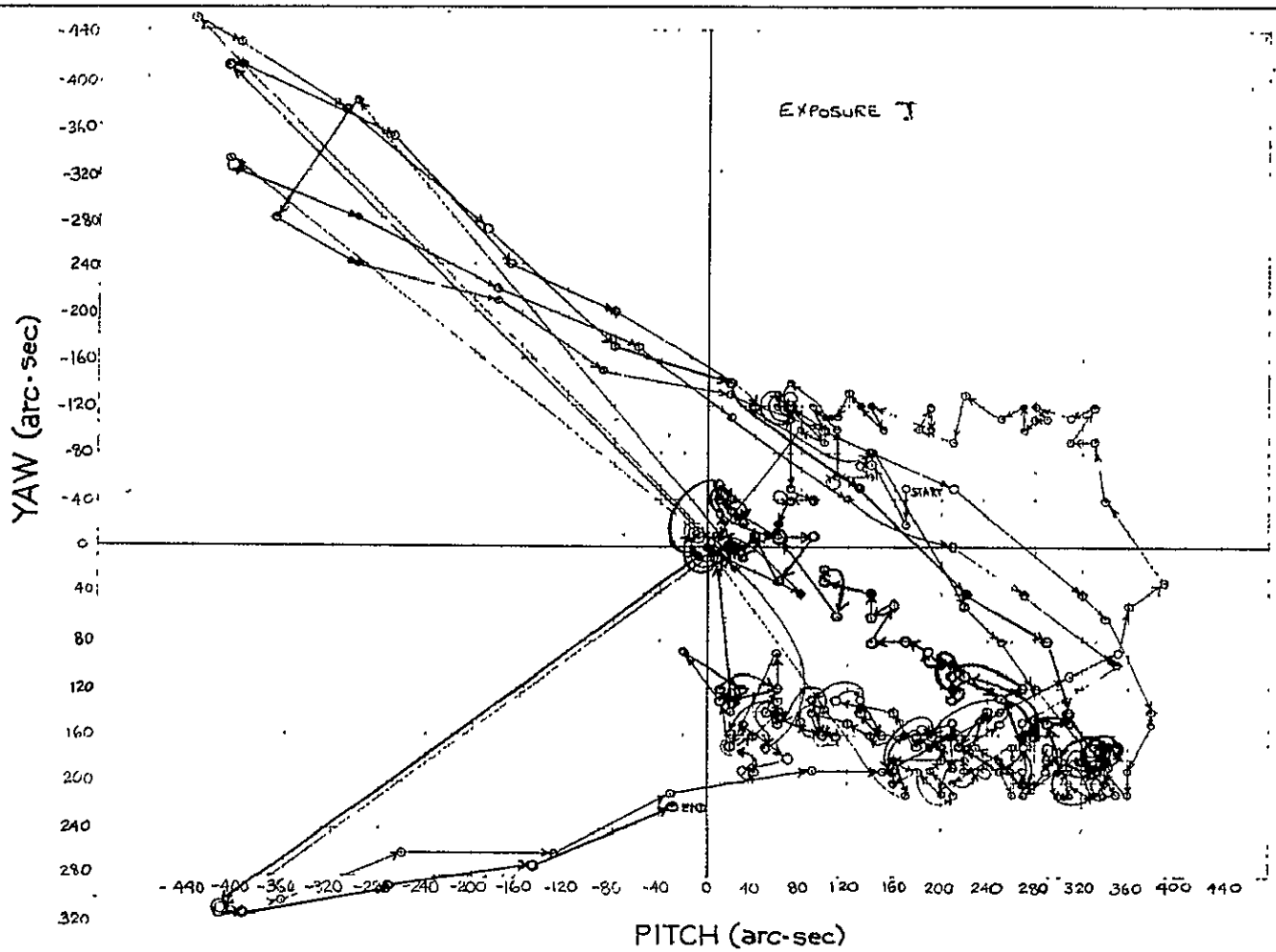

Figure 2.5 Angular displacement of the optical axis during Exposure I. Duration = 33.8 sec.

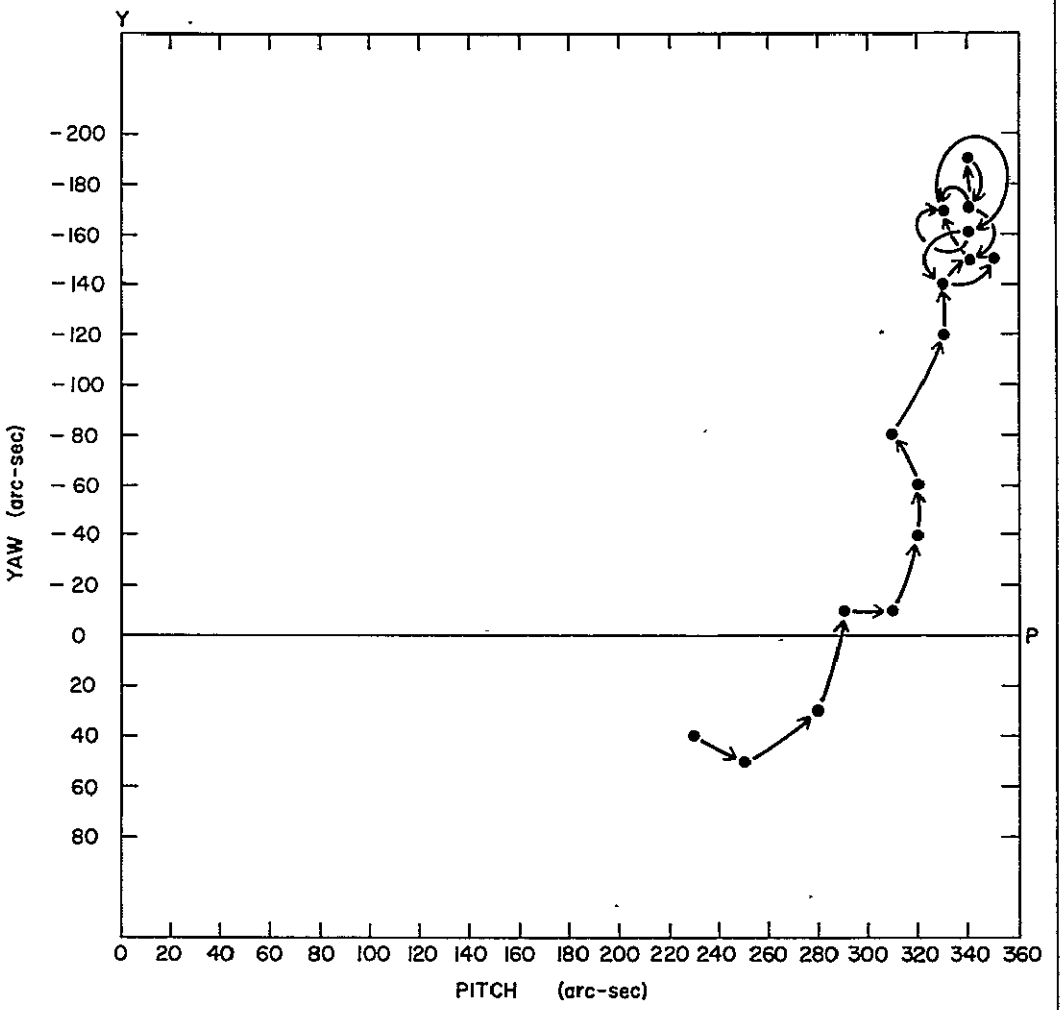

Figure 2.6 Angular displacement of the optical axis during Exposure II. Duration = 2.2 sec.

The various stages and procedures in the analysis are outlined below.

First the variation in photographic density across the exposure is measured using a microdensitometer. The resulting two-dimensional, color coded, isodensitometer tracing (IDT) of the parylene exposure is shown in Figure 2.7. The contours of photographic density must be calibrated in terms of the incident energy. This is accomplished by preparing a calibration film which contains a series of steps produced by a known number of aluminum $K\alpha$ X-rays. Each step of the calibration film is exposed to twice the number of photons as the previous step. The highest step is chosen to have the maximum density recordable by the film. In general the calibration strips contain 10 or more steps. After converting the number of photons to energy, we can obtain the relationship between net measured photographic density and incident energy. Each solar X-ray exposure is developed together with a calibration strip to prevent uncertainties arrising from differences in the development process. Then by scanning the calibration strip at the same time as the X-ray image, the density contours can be related to the energy in ergs deposited on the film.

The IDT shown in Figure 2.7 was produced by scanning the parylene exposure with a 50 by 50 μ pinhole and a magnification of 10:1. The areas of constant density shown on this IDT have been integrated using a compensating polar planimeter to obtain integrals of the total deposited energy as a function of area. The results of these integrations are shown in Figure 2.8. It is seen that the whole sun, including the corona, deposited a little less than 1 erg of X-ray energy on the film during the 2 second exposure. We can convert this energy into the incident flux in front of

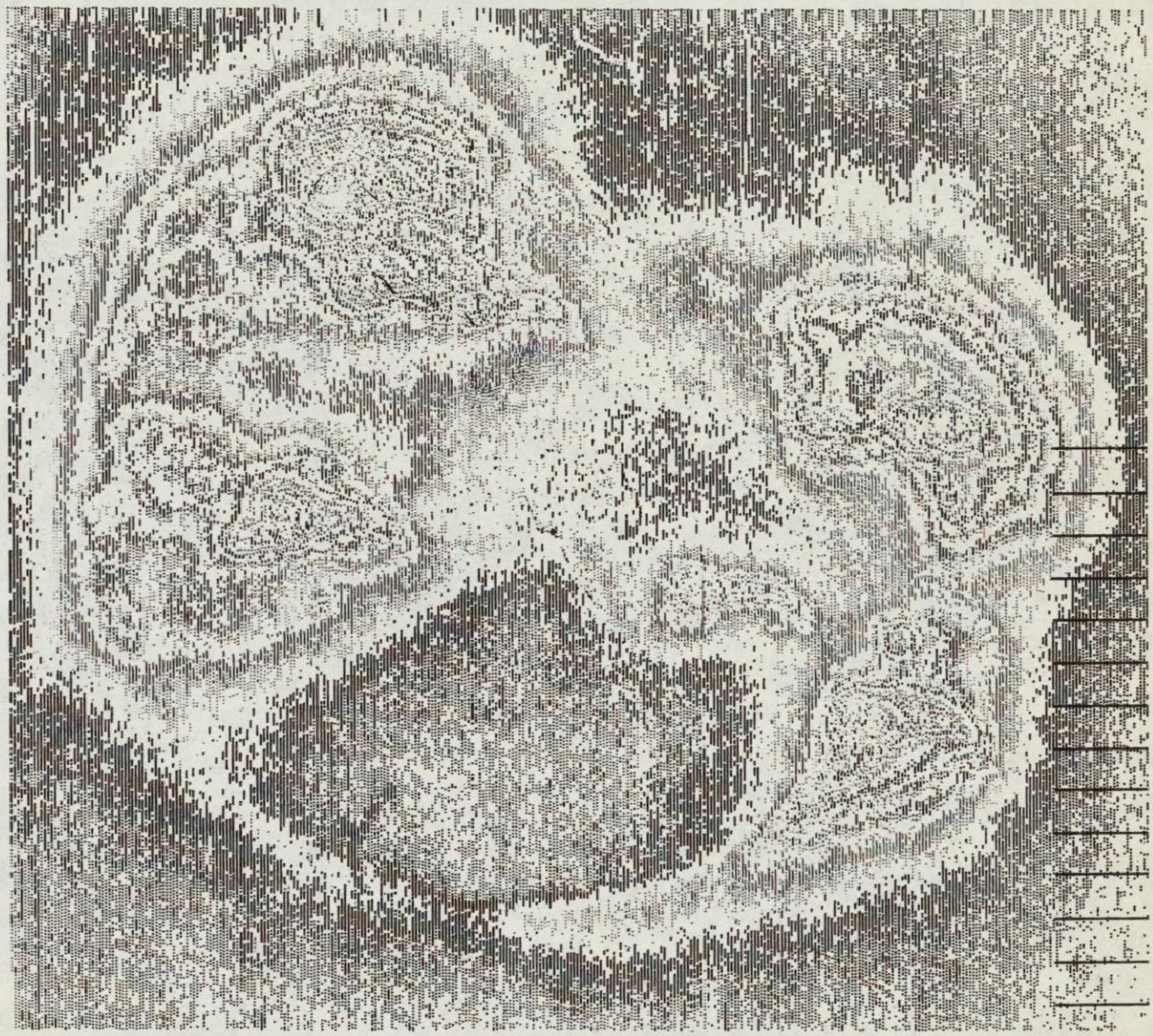

Figure 2.7 Two-dimensional isodensitometer tracing of Exposure II.

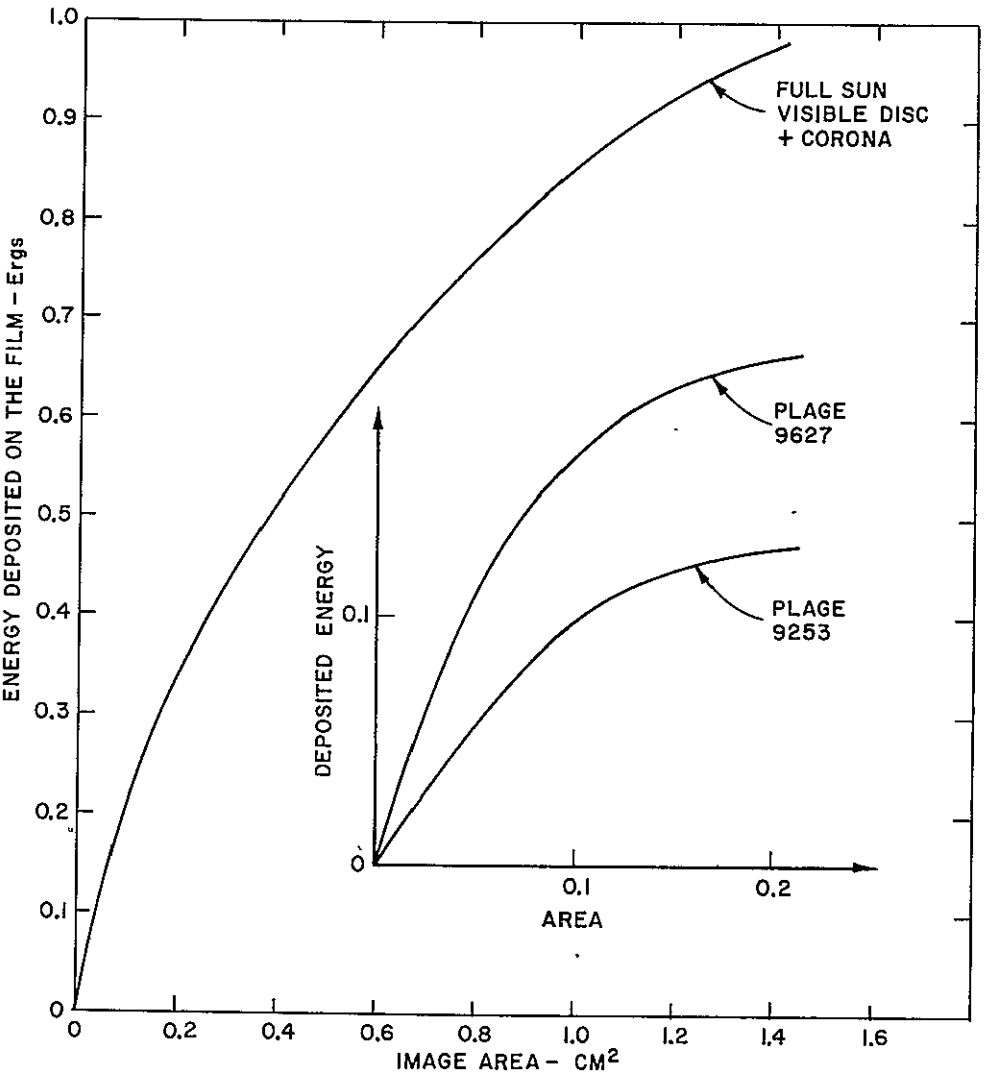

Figure 2.8 Integrals of the energy deposited on the film as a function of area for Exposure II.

the telescope by folding in the wavelength response of the telescope and the parylene filter. These curves are shown in Figure 2.9. After performing the calculation we obtain a value for the flux in the wavelength band 3.5 to 25 Å of 3.6×10^{-2} erg cm^{-2} sec^{-1}. Thus the sun was emitting energy at the rate of 1×10^{26} erg sec^{-1}, in this wavelength band at this time.

The energy emitted by the sun is the summation of the energy emitted by the several active regions. Integrals for two of these regions are shown in the insert of Figure 2.8. Region 9627 is the region which produced the subflare and is a young region, while region 9253 has been present for at least 5 solar rotations. The integrals from these and the other visible plages suggest that there may exist a differentiation with respect to age of the emission characteristics. Thus the central area is less pronounced in the older active regions and consequently they appear more diffuse than the younger regions. However because of the poor quality of the data no really firm statement can be made at this time.

In conclusion we note that the radiation from active region 9627 makes up slightly more than 20% of the total X-radiation of the sun although it occupies only about 10% of the area.

2.6 Structure of the Flaring Region

Comparison of the exposures obtained with the parylene and beryllium filters show the exponential nature of the emission, as most of the energy appears at wavelengths longer than the 13 Å cut-off of the beryllium filter. In fact the beryllium exposure contains little more than the bright point associated with the flaring region. Figure 2.10 shows a series of one-dimensional IDT scans across the flare normal to the direction of motion of the optical axis. The scans were made at a magnification of

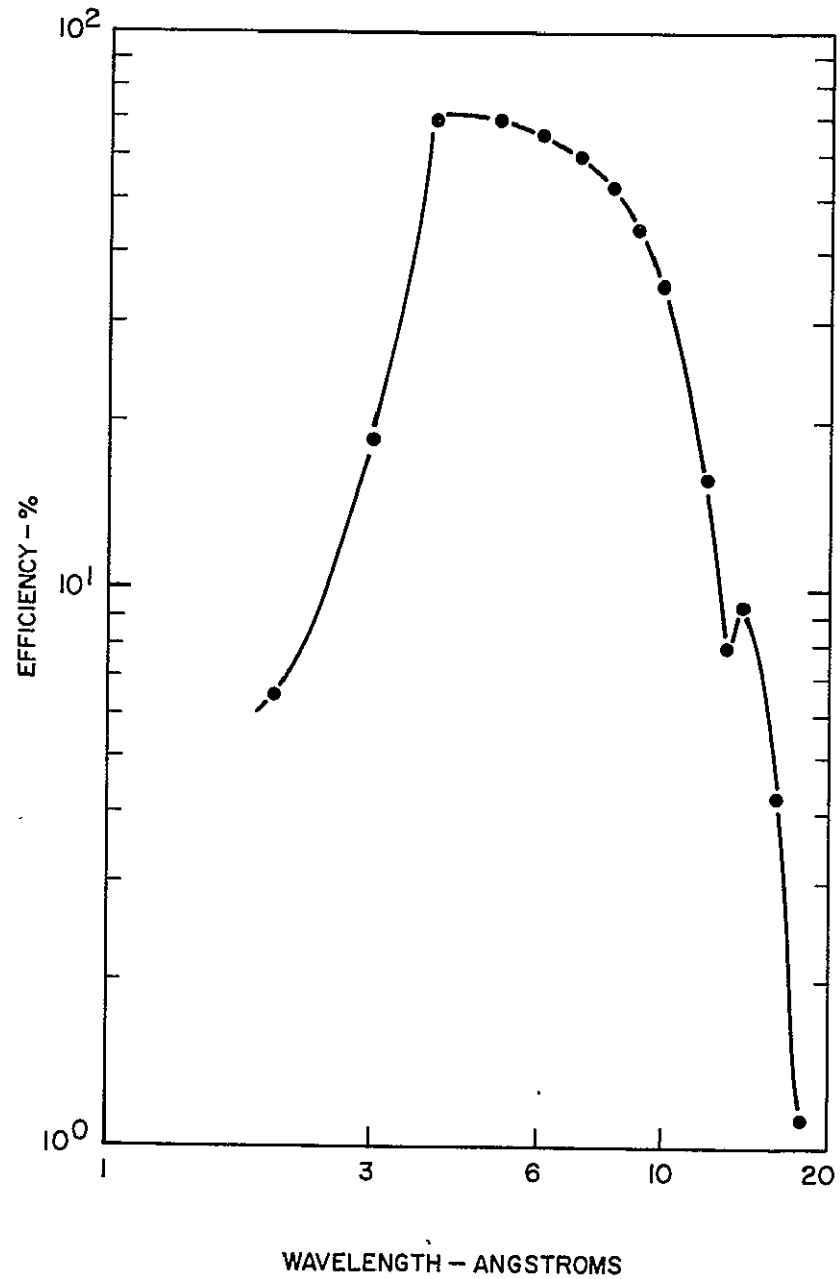

Figure 2.9 Wavelength passbands of solar rocket telescope.

(a) Telescope and 1/2 mil Beryllium filter.

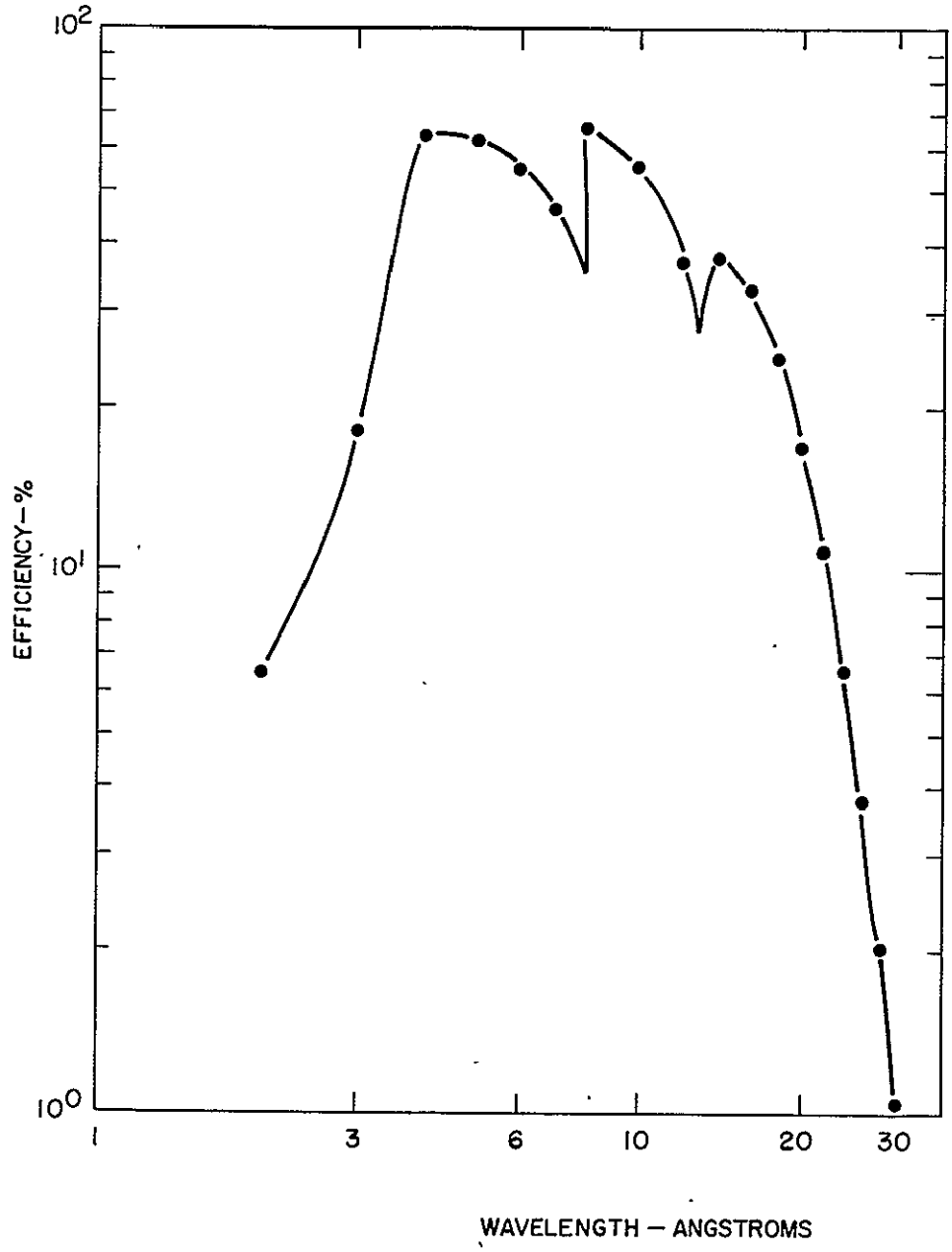

Figure 2.9 Wavelength passbands of solar rocket telescope

(b) Telescope and Parylene filter.

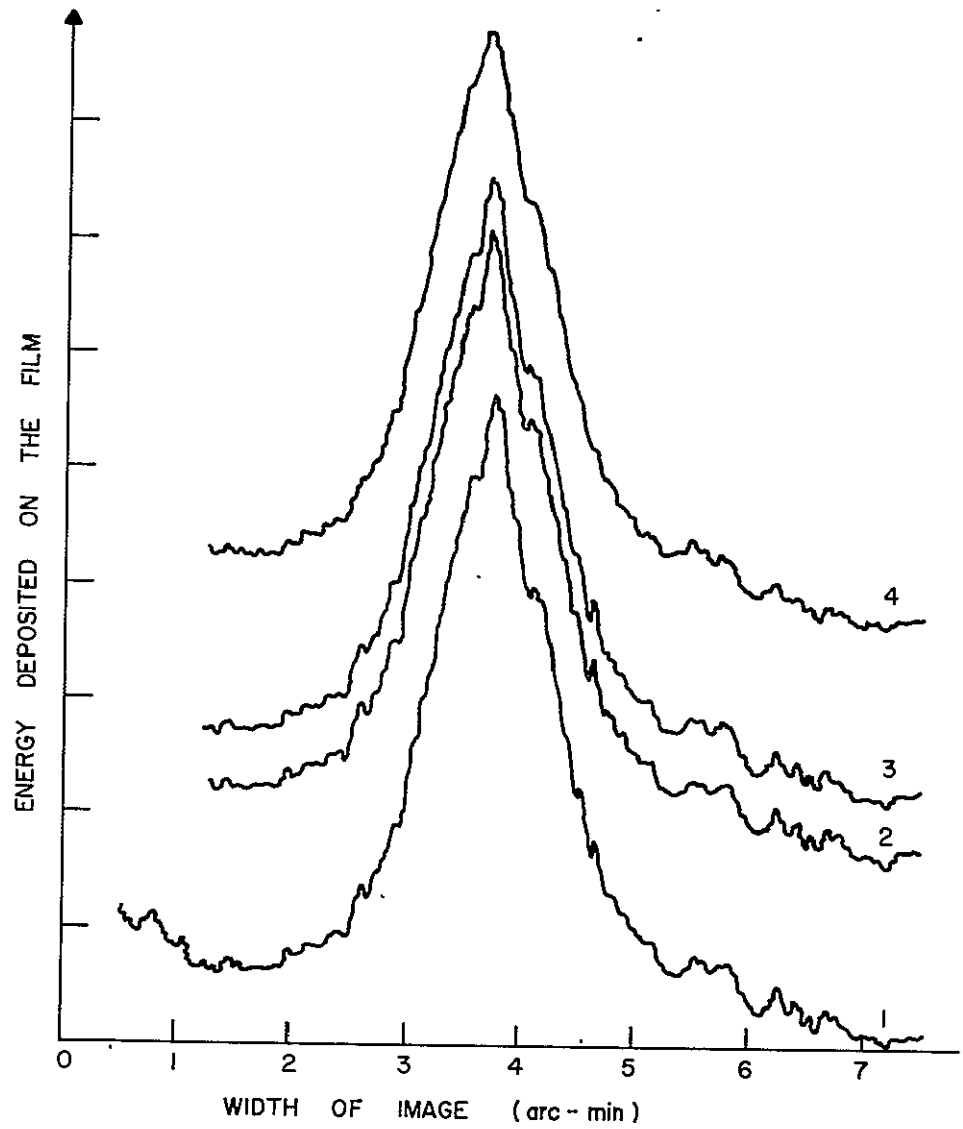

Figure 2. 10 One-dimensional isodensitometer scans of the flaring region visible on Exposure V.

50:1 with a pinhole of dimensions 20 by 200μ.

The full width at half maximum of the resulting distribution is approximately 1 minute of arc. However, our experience suggests that this width may arise almost entirely from the scattering function of the telescope and that the flaring region itself was probably less than 5 arc-seconds wide.

2.7 Solar X-ray Line Spectra

The final 3 exposures taken on the March 15 flight had a transmission grating interposed between the telescope and the image plane. Of these one was lost due to a catastrophic failure of the parylene filter. The other 2 were taken with a 1/2 mil beryllium filter and both of these had their images severely degraded by the rocket motion. Consequently it was impossible to interpret their images.

3.0 EXPERIMENTAL MODIFICATIONS, TESTING AND ALIGNMENT

3.1 Experimental Hardware

The hardware for NASA Aerobee rocket 4.263 CS payload was constructed under NASA Contract NASW-1555 and is described in the final report for that contract (Document ASE-1953). A list of the major systems of the payload follows:

a. Nose cone eject mechanism and support ring.

b. Mirror protection device mechanism.

c. Solar Capture and Tracking (SCAT) system fine eyes.

d. Grazing incidence X-ray mirror, focal length 52", with visible light lens, filter and pin hole apertures.

e. Mirror-Camera optical mounting system.

f. Movable X-ray transmission grating.

g. Electronics panel.

h. Instrumentation panel.

i. Single reflection light baffle.

j. Twelve frame rotating drum, camera and adjustable mounting support.

After launch the experiment was controlled by a central processor mounted in the electronics panel. Two Haydon chronometrically governed DC interval timers were used to provide the timing sequence for the camera exposures and to provide the command to position the grating at the end of the ninth exposure.

The commands for ejection of the nose cone and starting the timers were supplied by the ACS (SCAT) system. The eject command was given immediately after erection and stabilization of the vehicle at T + 81 seconds. The start programmer command to actuate the timers and camera was given after the fine eyes had pointed the payload at the sun. This occurred at T + 113 seconds.

The complete sequence of events in chronological order with the appropriate T + time is given in Table II.

The command to close the mirror protection device was given by the timer at severance from the instrumentation system. The time of command was T + 300 seconds and it was also used to shut off power to the programmer and lock the camera in position.

3.2. Repairs and Modifications

After the initial flight in this series, 4.209 CS, the payload had landed on the side of a cliff. The rocket casing had received a number of severe scratches and dents and the mirror protection device was also severely damaged. However post flight inspection showed very little internal damage and no degradation of the mirror performance was observed.

On return of the payload to AS & E the mirror protection device, which had been designed to completely close the front of the payload cylinder at severance to prevent damage to the mirror on impact, was completely rebuilt. The dents in the rocket skin were knocked out and it was decided to replace the 2 parylene filters with 1/8 mil mylar filters, coated with 2200 Å of aluminum, as one of the parylene filters had ruptured during the ascent stage of flight 4.209 CS. Some minor modifications were made to the exposure times based on the experience gained from the initial flight (Table III).

These changes were completed by the end of April 1968 and the payload was delivered to NASA-GSFC on May 1, 1968 for integration and testing. The following tests were performed in the sequence recorded below.

May 1, 1968	Arrived at NASA-GSFC, installed flight eyes and instrumentation panel, set up and checked out

TABLE II

Sequence of Events for Aerobee 4.263 Flown on June 8, 1968

T + Time	Function	Exposure
0	Launch	
52	Burn out complete	
52	Coast-Release lockout relay	
64	Despin	
66	Erect	
81	Eject Nose-End stabilize	
83	Eject Nose-Roll stabilize	
93	Pitch	
103	Fine lock	
113	Start programmer (Timer I)	
115	22 sec. exposure	1
137	Timer II start	
138	2 sec. exposure	2
140.5	6 sec. exposure	3
147	19 sec. exposure	4
166	2 sec. exposure	5
172	6 sec. exposure	6
178.5	18 sec. exposure	7
196	2 sec. exposure	8
203	6 sec. exposure	9
209	Grating released	
210	6 sec. exposure	10
216	22 sec. exposure	11
238	52 sec. exposure	12
300	Severance	
	Stop programmer	
	Lock Camera	
	Engage Mirror protection	

TABLE III

Exposure Sequence for Aerobee 4.263 Flown on June 8, 1968.

Exposure	Film	Filter	Trans-mission Grating	Exposure Time (sec)
1	103-0 un-tc	1/2 mil Beryllium	No	22
2	Pan x tc	2 mil Beryllium	No	2
3	Pan x tc	1/2 mil Beryllium	No	6
4	Pan x un-tc	1/2 mill Beryllium	No	19
5	Pan x tc	1/2 mil Beryllium	No	2
6	Pan x un-tc	1/8 mil Mylar	No	6
7	103-0 un-tc	1/10 mil Steel	No	18
8	Pan x tc	Visible	No	2
9	Ilford Special	1/8 mil Mylar	Yes	6
10	103-0 un-tc	1/2 mil Beryllium	Yes	6
11	103-0 un-tc	1/2 mil Beryllium	Yes	22
12	103-0 un-tc	1/2 mil Beryllium	Yes	52

Films labelled tc or un-tc are with or without a protective gelation layer (top coating) respectively. The Mylar filters were coated with about 2200 Å of aluminum to stop the passage of visible light.

	equipment. Ran preliminary integration test. Set up for vibration testing of the ACS. Ran vibration tests at standard test levels. Inspected and reran integration test.
May 2, 1968	Moved to Stabilization and Control Branch building and aligned eyes to optical axis. No new adjustments were necessary.
May 3-6, 1968	Ran air bearing tests and final integration.
May 7, 1968	Packed equipment and returned to AS&E.

3.3 Description of Tests

The following paragraphs describe in slightly more detail the testing performed at GSFC.

Integration Tests

The payload was mated with the Attitude Control System (ACS) and the instrumentation panel. A complete simulated flight was conducted and data recorded by the GSFC telemetry ground station. A transmitter-receiver link was employed (i.e. not a hard line link). No major problems were encountered during the running of this test. The ACS was then subjected to vibration testing and after visual inspection a second integration test was carried out. All systems, including the squib operated mechanisms worked normally.

Alignment of Eyes to Payload Optical Axis

The instrument had been designed with stringent tolerances to allow the pointing eyes to be hard mounted to the aperture plate without the use of shims. This was verified by optical testing. The mirror and camera had been previously aligned at AS&E. The effects of the vibration test on the mirror and camera alignment were checked by taking photographs with the payload camera of

the images produced by the solar simulator. These tests confirmed that the camera film plane was still aligned with respect to the mirror focal plane.

Vibration Testing

As the flight was a reflight of previously tested equipment without major modifications, some of the vibration testing requirements were waived by GSFC.

Final Inspection

After the payload was returned to AS&E, it was disassembled and a detailed inspection was performed. The payload was then reassembled and shipped to White Sands Missile Range (WSMR).

4.0 FLIGHT OF 4.263 CS

The payload, equipment and personnel arrived at WSMR on May 11, 1968, to prepare for launch which was scheduled to occur between May 18 and June 8, 1968.

After arriving at WSMR, the payload was checked out electrically and preparations were made for checking the camera focal plane. Procedures were arranged for taking photographs with the payload camera of the sun and of a laser beam that was set up at a temporary station 8.8 miles from the camera. These photographic tests were performed periodically throughout the 2 week period prior to mounting the rocket in the tower.

On May 14 the flight mirror was cleaned and the grating mechanism was installed. Functional and horizontal testing was done on May 15. During the horizontal test only one side of the grating mechanism operated. This necessitated replacing the negator spring for this half of the grating mechanism. Both sides then operated successfully.

The rocket and payload were placed in the launch tower on May 17 and the vertical test was completed with all systems operating satisfactorily. After completion of the test it was learned that the launch had been postponed until May 25, 1968. A second vertical test of the ACS(SCAT) was performed on the following day. After this test the camera was removed and prepared for flight by installation of flight film and filters.

Tests of the organic flight filters were not completely satisfactory. Since there was a delay in the launch schedule, new Mylar filters were prepared and tested at AS&E and hand carried to WSMR. These arrived on May 24 in time to be integrated with the camera and mounted in the payload prior to the first scheduled launch period.

It was hoped to launch 4.263 CS during a class 2 solar flare. Consequently the count down would be held at T-3 minutes until the project scientist was notified of such an occurrence by the staff at ESSA, who were coordinating the flare patrol and ground-based measurements. If at the end of 2 weeks such a flare had not occurred, the scientific criteria for launch would be relaxed.

The various countdowns prior to eventual launch were as follows (note times are Mountain Daylight Time unless otherwise specified):

May 25, 1968	Count held from 1330 to 1830 M.D.T. Cancelled due to high shifting winds.
May 26, 1968	Count held at 0830 M.D.T. Count restarted at 1153 and T-30 sec for a class 3 flare, recycled to T-3 min. Cancelled at 1723 M.D.T.
May 27, 1968	Count held at 0830 M.D.T.; cancelled at 1145 M.D.T. due to conflicting range schedules.
May 28-30, 1968	Launch not scheduled.
May 31, 1968	Count held at 0830 M.D.T.; cancelled at 1735 M.D.T.
June 1, 1968	Count held at 0830 M.D.T.; cancelled at 1730 M.D.T.
June 3, 1968	Count held at 0830 M.D.T.; cancelled at 1705 M.D.T.
June 4, 1968	Count held at 1515 M.D.T.; cancelled at 1715 M.D.T.
June 5, 1968	Count held at 1515 M.D.T.; cancelled at 1730 M.D.T.
June 6, 1968	Count held at 1515 M.D.T.; cancelled at 1730 M.D.T.
June 7, 1968	Count held at 1200 M.D.T., recycled at 1415 M.D.T. due to conflicting range schedules. Count restarted and held at 1500 M.D.T. and finally cancelled at

	1645 M.D.T. due to high winds.
June 8, 1968	Scientific criteria relaxed as last available date for launch. Count held at 0830 M.D.T. The project scientist was alerted at 1137 M.D.T. to the occurrence of an Hα flare by the co-ordinating ESSA scientist and ordered the resumption of the countdown. Launch took place at 1140 M.D.T.

The launch at 1140 M.D.T., or 1740 U.T., was successful as all AS&E and NASA-GSFC systems operated correctly. An apogee of 93 miles was achieved and severance occurred at T + 300 sec. The rocket had been launched during the occurrence of a large 1N flare of the parallel ribbon kind. The onset of the flare was at approximately 1732 U.T., reached the maximum development at about 1745 U.T. and lasted about 1.5 hours. The rocket, launched at 1740 U.T., acquired the sun at 1742 U.T., and obtained exposures until 1745 U.T. The pointing control, developed by the Sounding Rocket Branch of GSFC achieved the unprecedented accuracy of $\pm$ 1 second of arc jitter throughout all of the exposures.

5.0 POST FLIGHT ANALYSIS AND RECOVERY

The payload was recovered at about 1500 M.D.T. the same day. It had landed in open country with no observable external damage. The flight films were recovered and returned immediately to AS&E for development. Later the payload was returned to AS&E and inspection showed no internal damage. Both of the mylar filters had survived the flight and no degradation in the performance of the mirror was observed.

6.0 FLIGHT FILMS FROM 4.263 CS.

The flight films have been developed and are presented in Figure 6.1 through 6.12. The main scientific result obtained was that structural features only a few arc-seconds in extent were observed in the X-ray flare for the first time. The photographs also show X-ray emitting regions associated with plages and the general X-ray coronal emission. Spectral data were acquired by means of broad band filters; dispersed spectra of individual active regions were also obtained using a slitless spectrograph.

The following general conclusions can be made from these photographs:

1. There is a one to one correspondence between centers of X-ray emission and centers of activity evidenced by correlations between the X-ray photographs and H_α, CaK and photospheric magnetic field data.

2. The general outline of the X-ray regions very closely resembles the outline of the H_α regions.

3. The X-ray emitting regions show a three-dimensional structure extending above the active regions which is not seen in H_α photographs.

4. This three-dimensional structure, which extends to considerable height in the corona, often takes the form of loops connecting portions of the same active region or of different active regions. The configuration of the plasma appears to be governed by the magnetic field and is complex. This complexity of the configuration at the coronal level is likely to facilitate the triggering of instabilities.

5. The slitless spectrometer technique proved able to

record the spectra of individual active regions. The preliminary analysis indicates that the spectra associated with the flare are measureably harder than most of the other active regions, and contain a MgXI line at 9.2 Å.

6. The X-ray component of the solar flare is highly structured. This fact eliminates models which are based on an extended diffuse cloud of radiating plasma. The general appearance of the X-ray flare is of an ordered filamentary structure with characteristic dimensions of the order of 10^4 km.

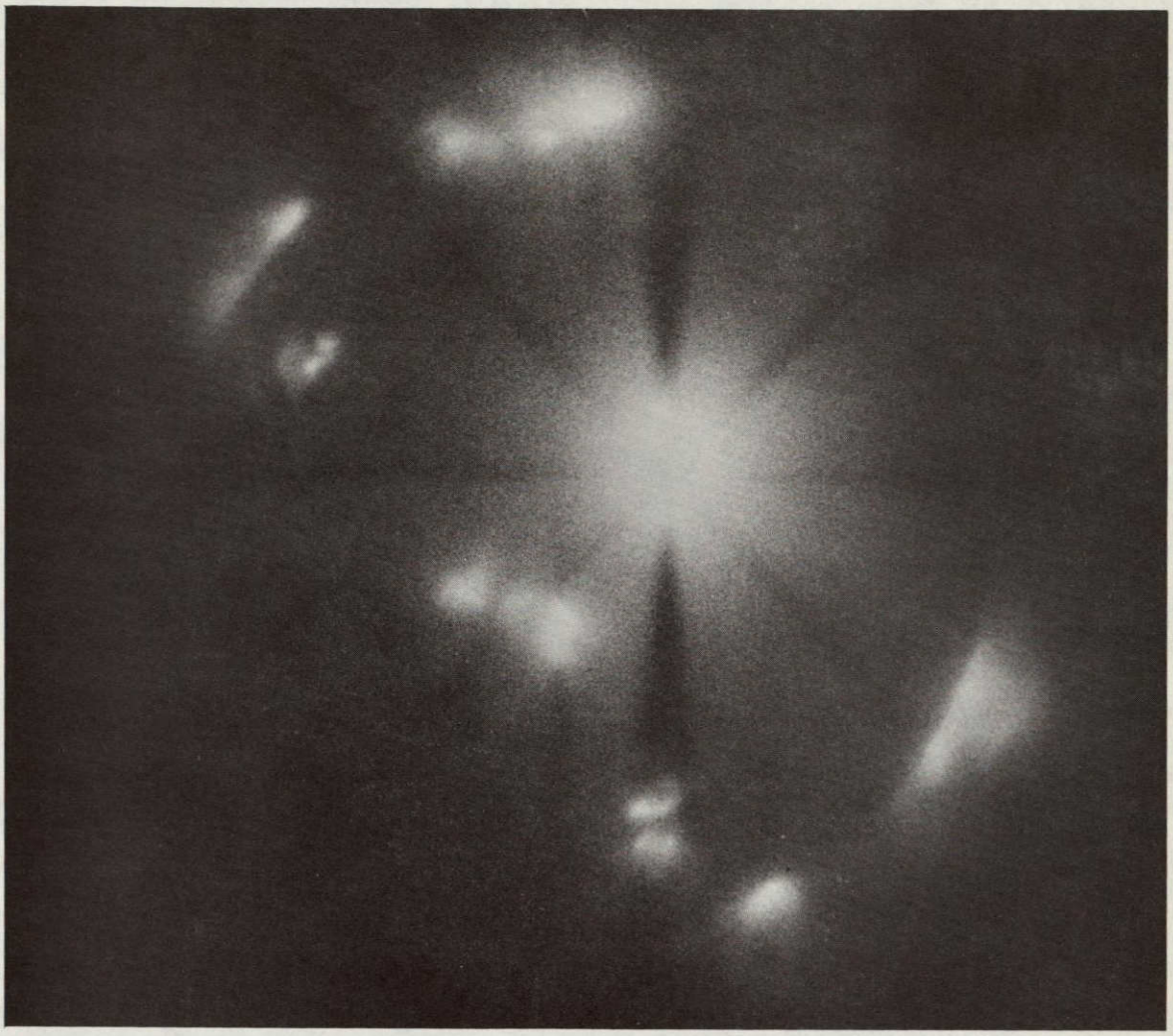

DZ-060

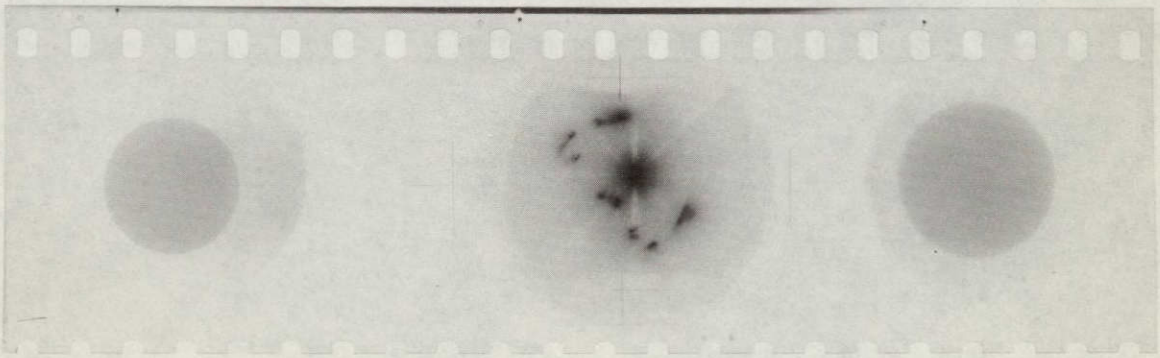

Figure 6.1 Exposure I June 8, 1968 (see Table III)

NOT REPRODUCIBLE

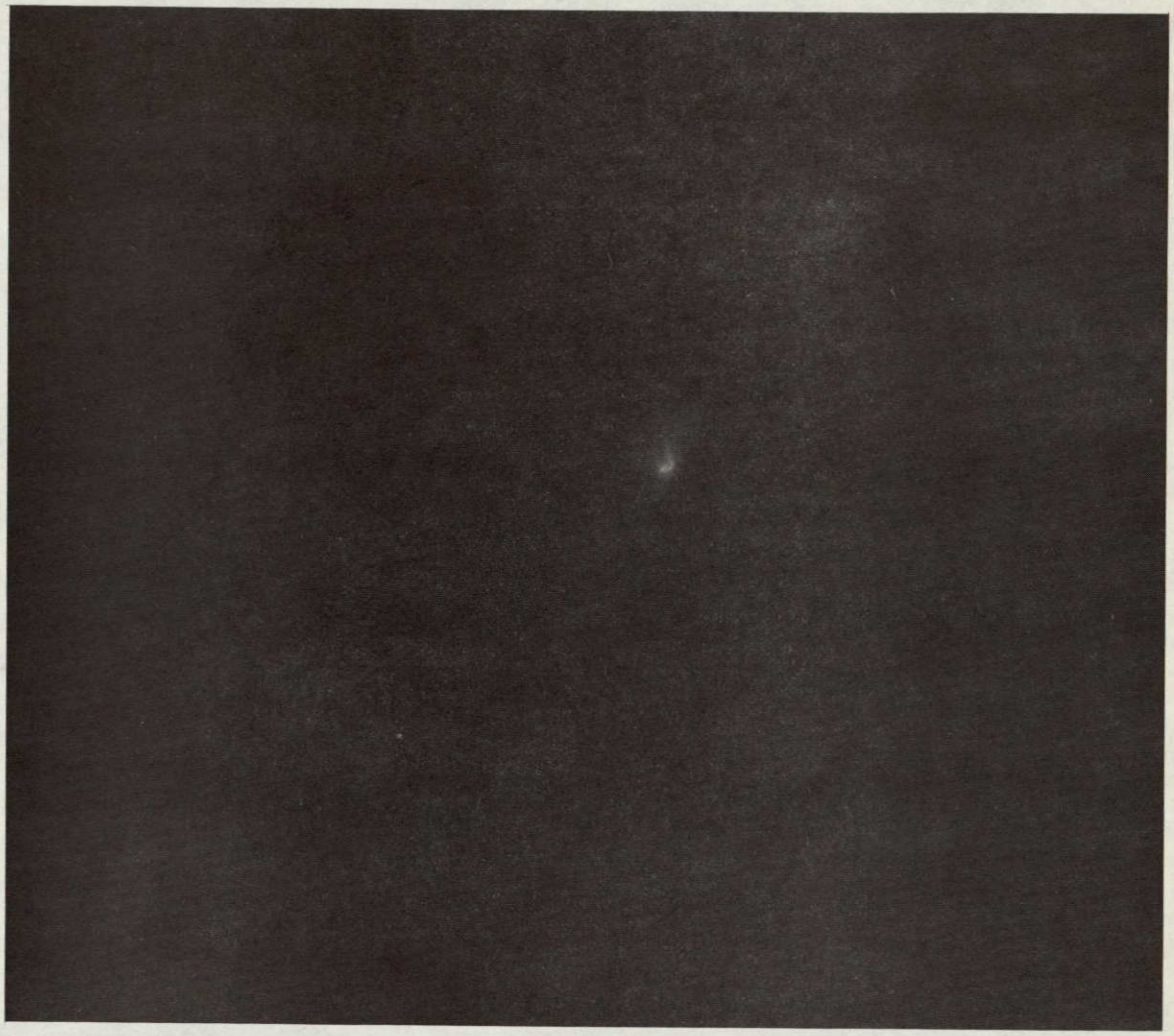

DZ-061

Figure 6.2 Exposure II June 8, 1968 (see Table III)

DZ-062

Figure 6.3 Exposure III June 8, 1968 (see Table III)

NOT REPRODUCIBLE

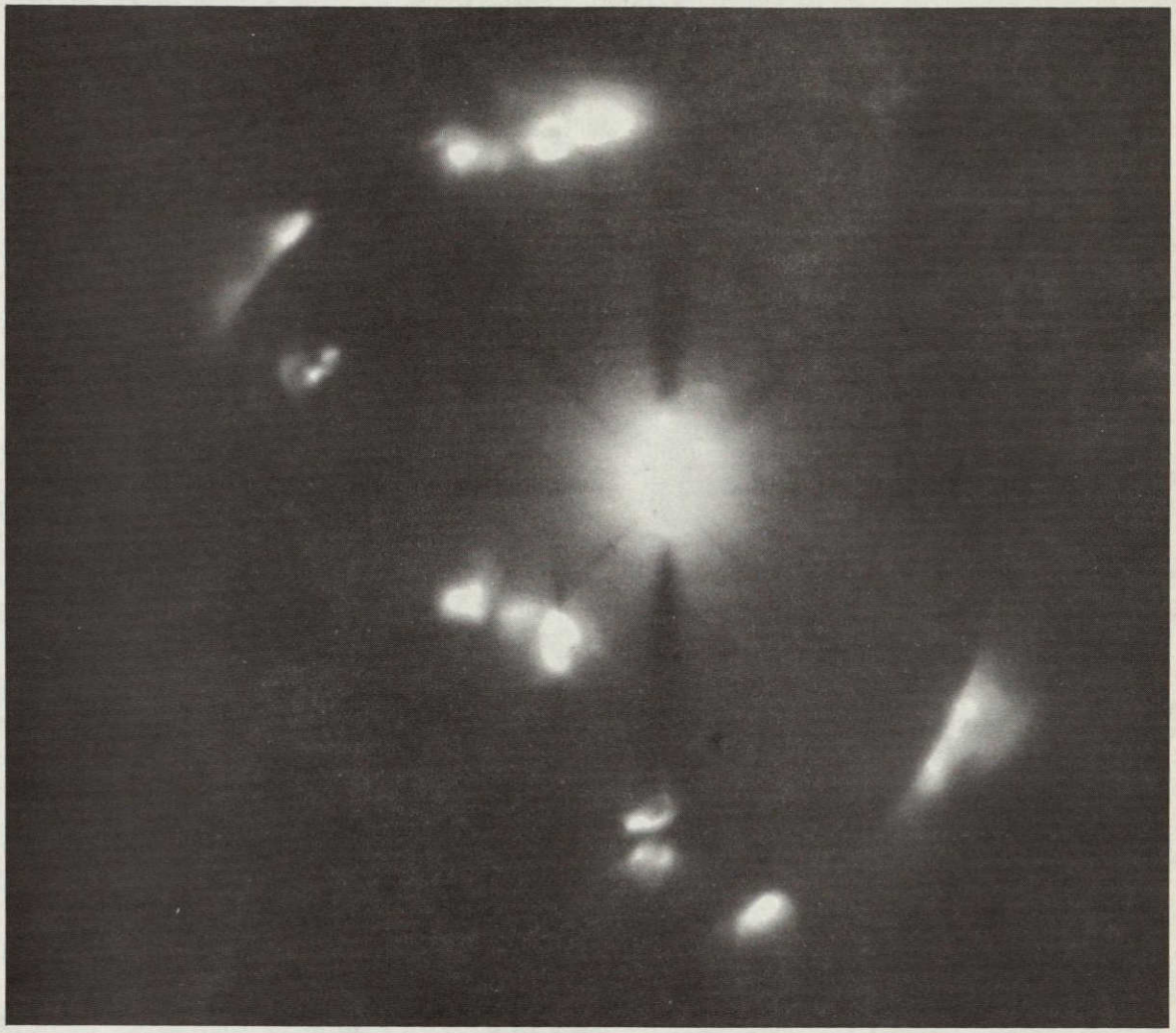

DZ-063

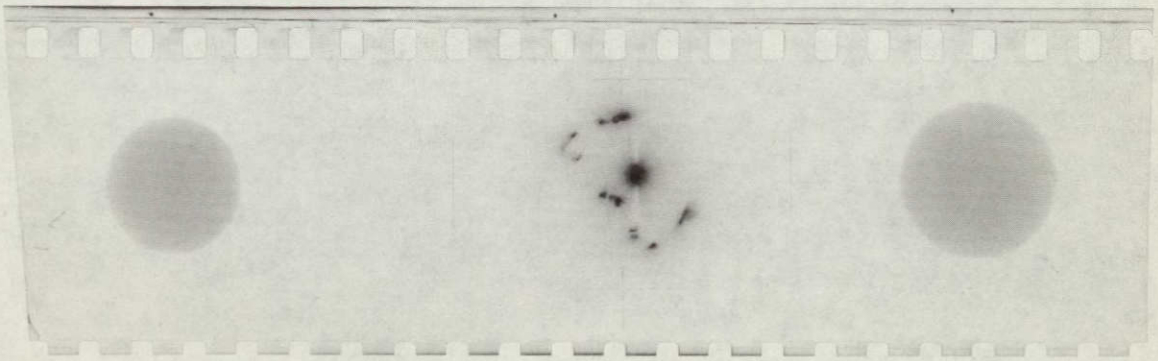

Figure 6.4 Exposure IV June 8, 1968 (see Table III)

DZ-064

Figure 6.5 Exposure V June 8, 1968 (see Table III)

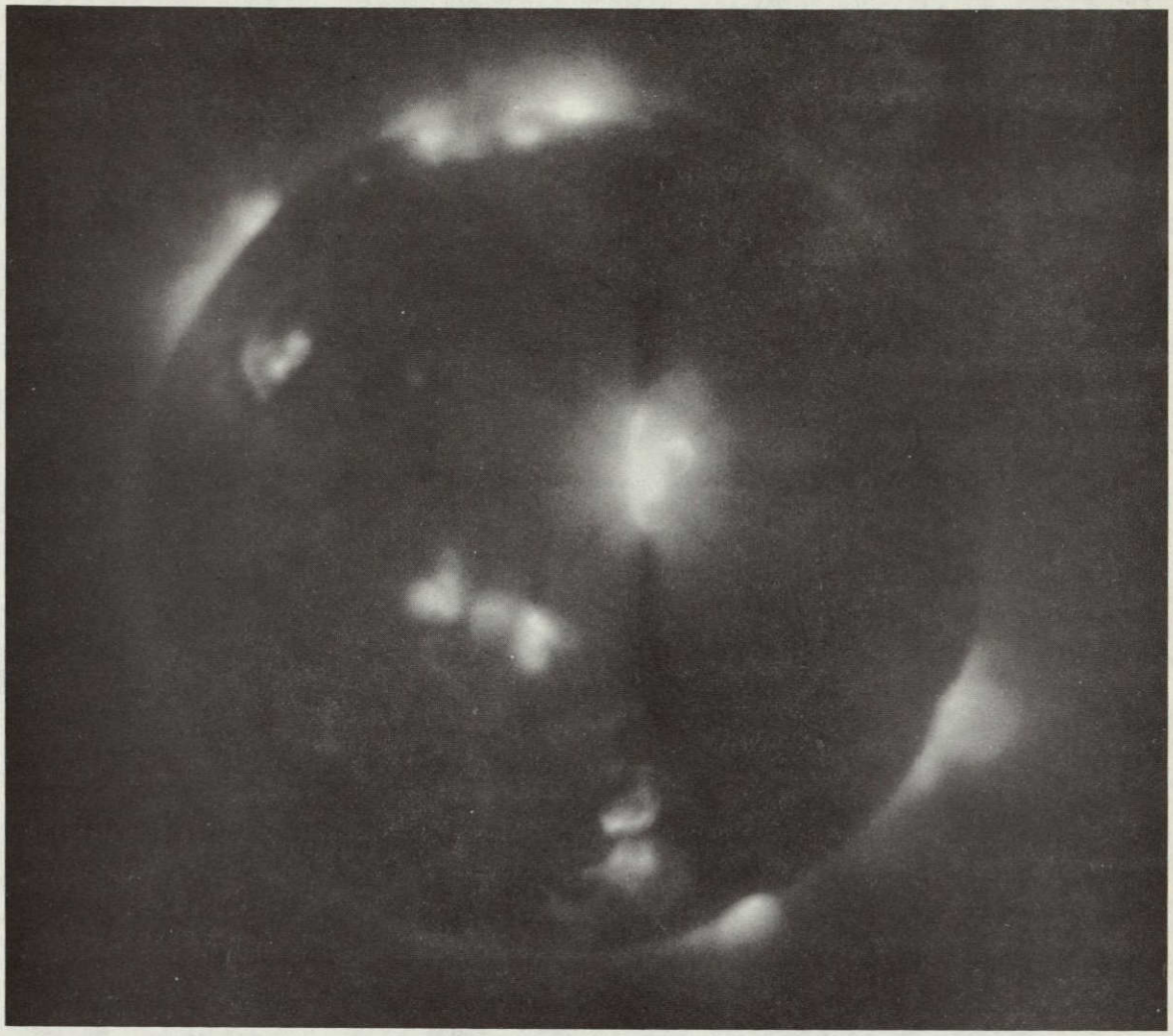

DZ-065

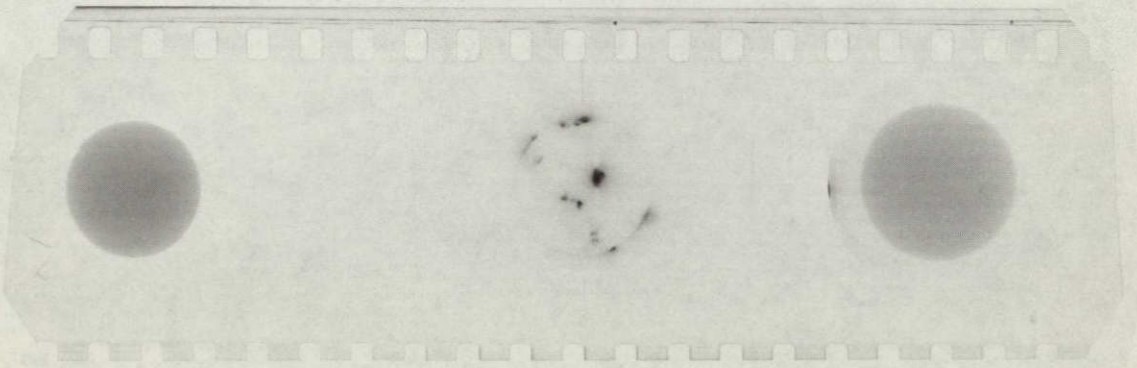

Figure 6.6 Exposure VI June 8, 1968 (see Table III)

NOT REPRODUCIBLE

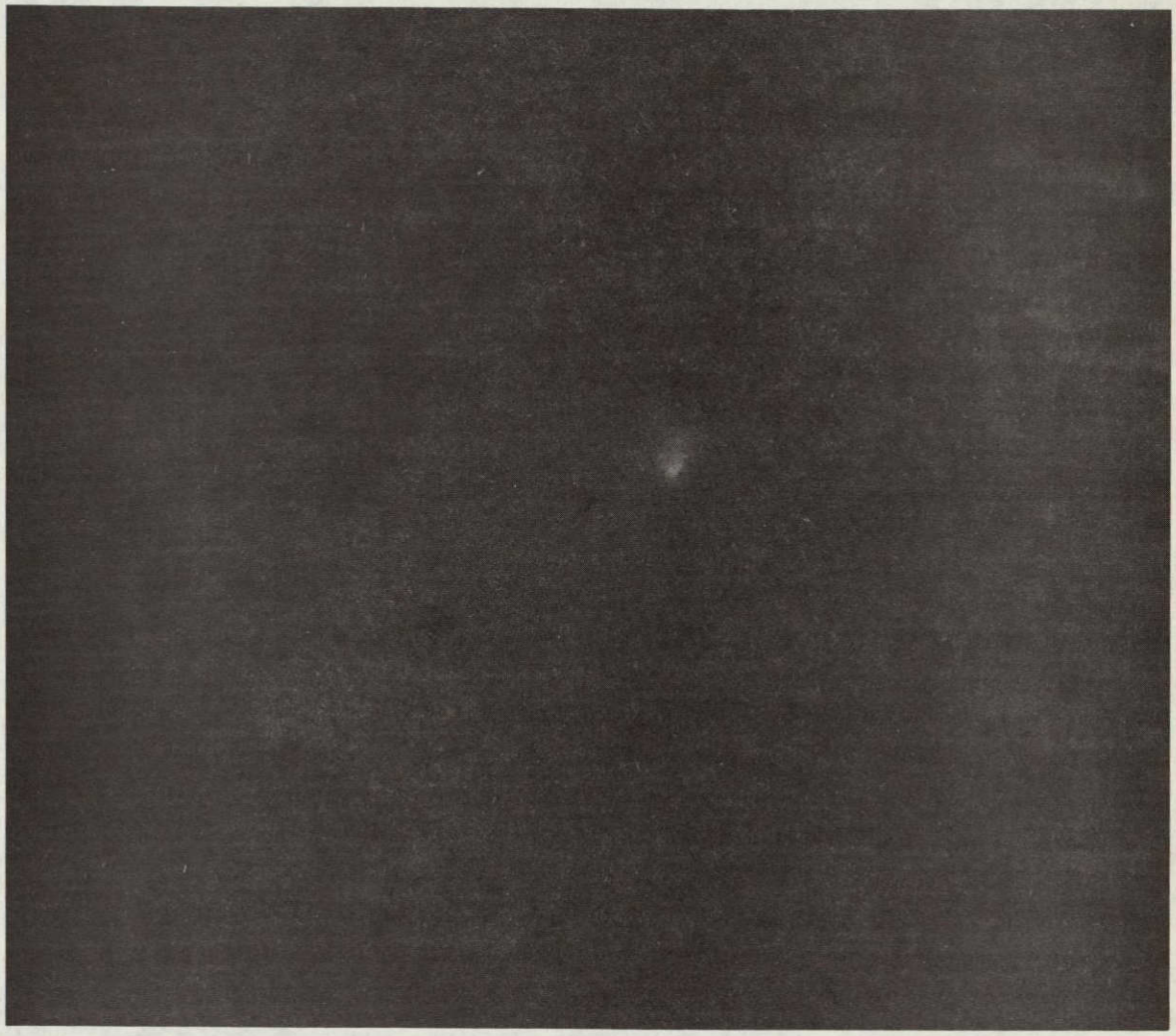

DZ-066

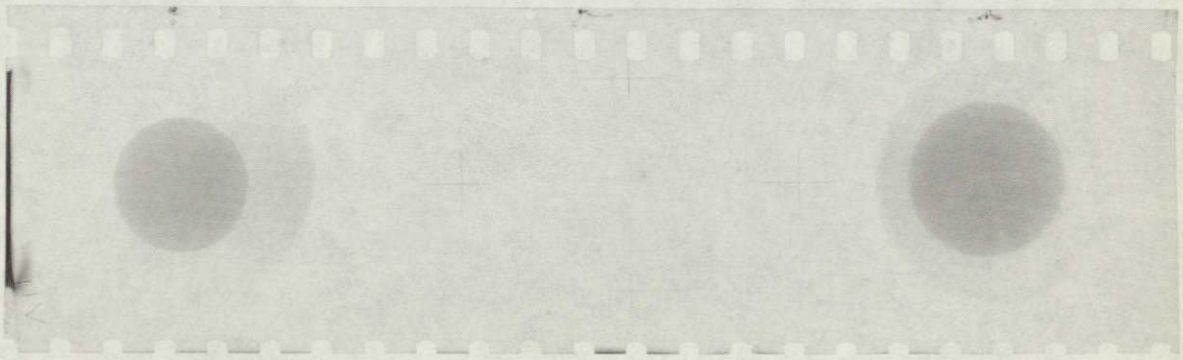

Figure 6.7 Exposure VII June 8, 1968 (see Table III)

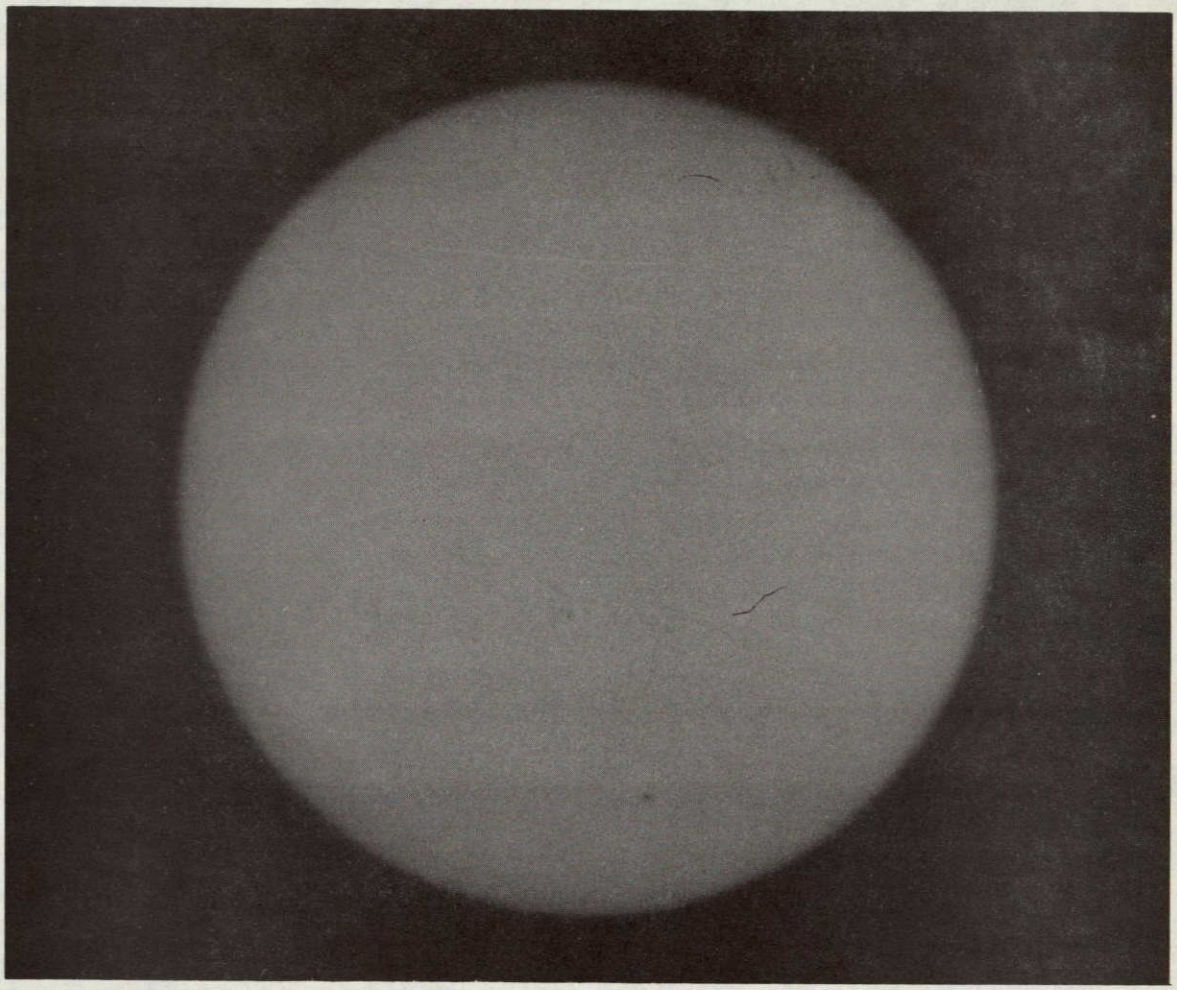

DZ-067

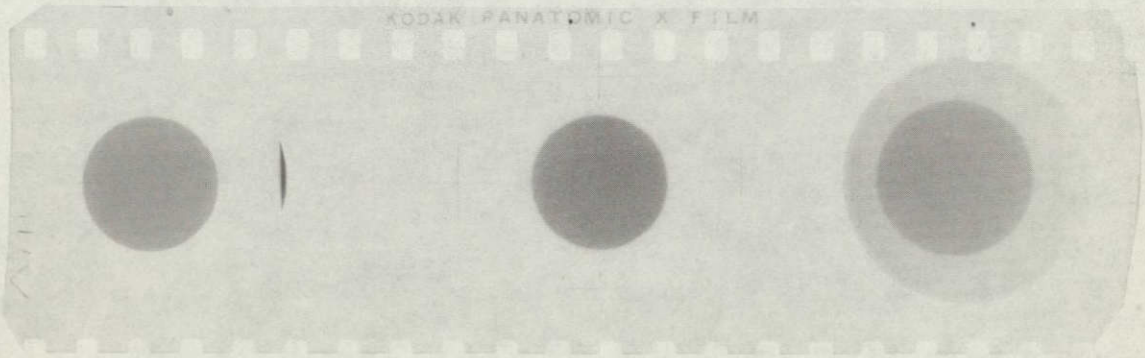

Figure 6.8 Exposure VII June 8, 1968 (see Table III)

NOT REPRODUCIBLE

DZ-068

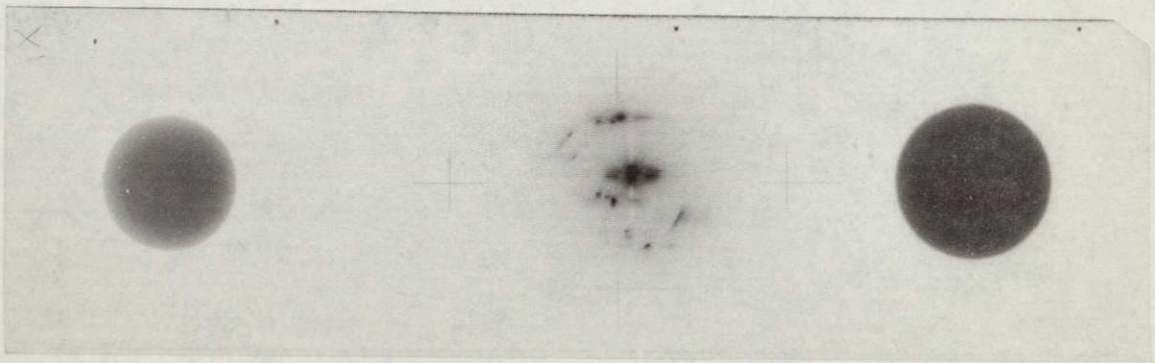

Figure 6.9 Exposure IX June 8, 1968 (see Table III)

NOT REPRODUCIBLE

DZ-069

Figure 6.10 Exposure X June 8, 1968 (see Table III)

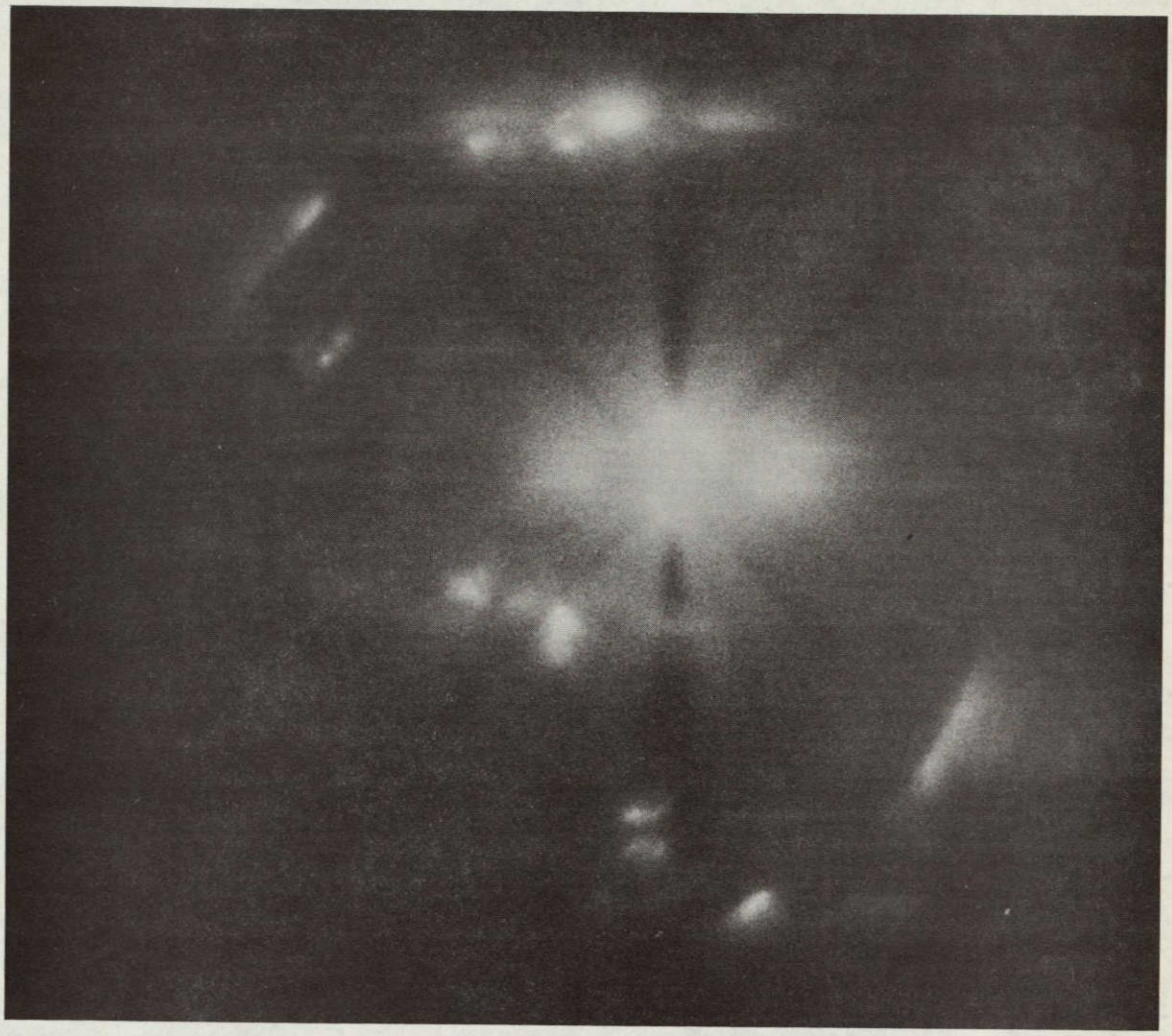

DZ-070

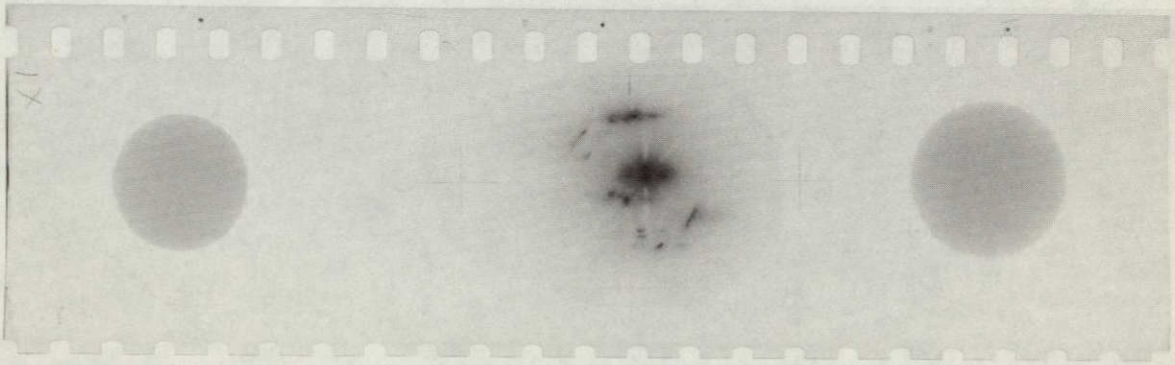

Figure 6.11 Exposure XI June 8, 1968 (see Table III)

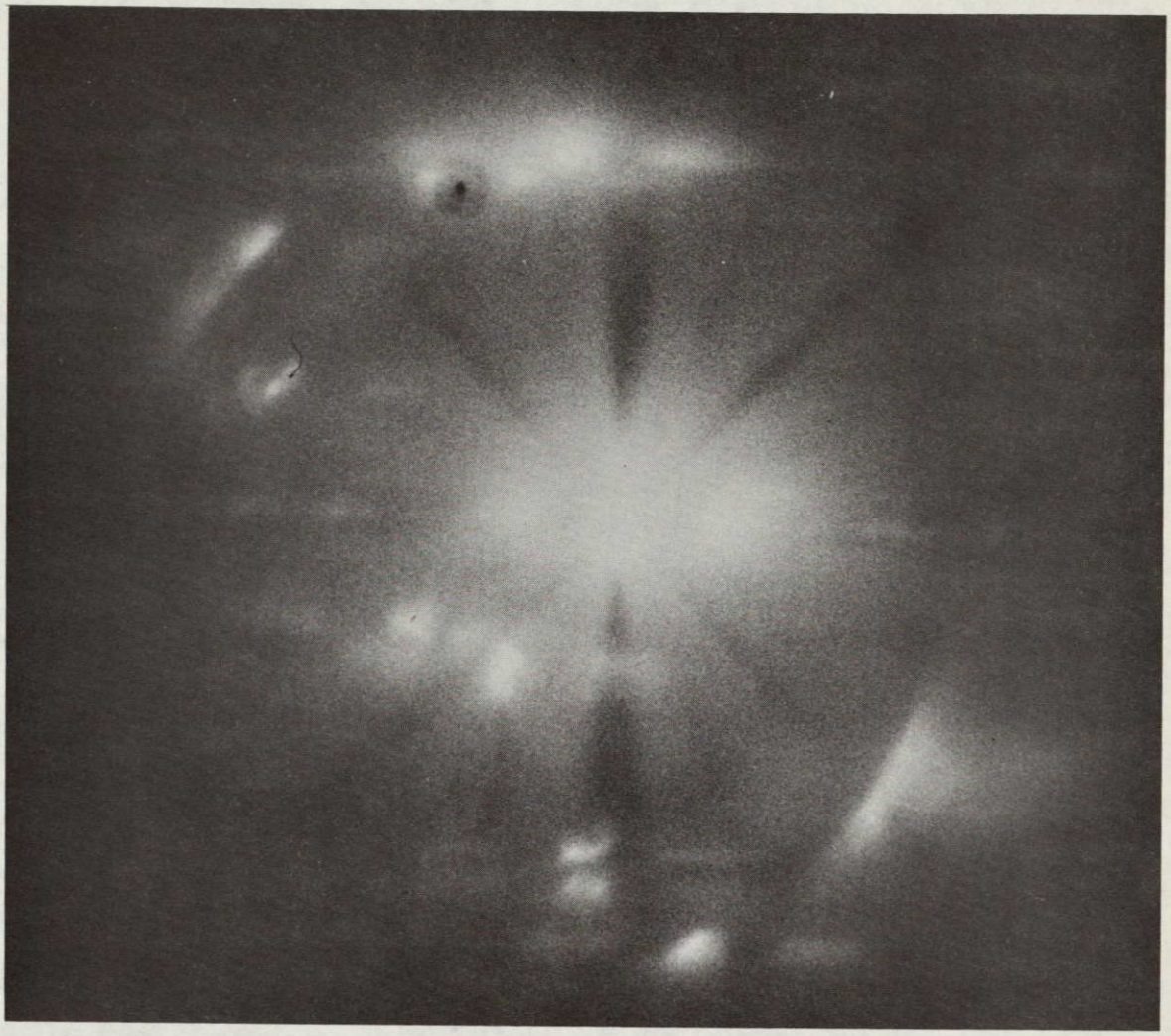

DZ-071

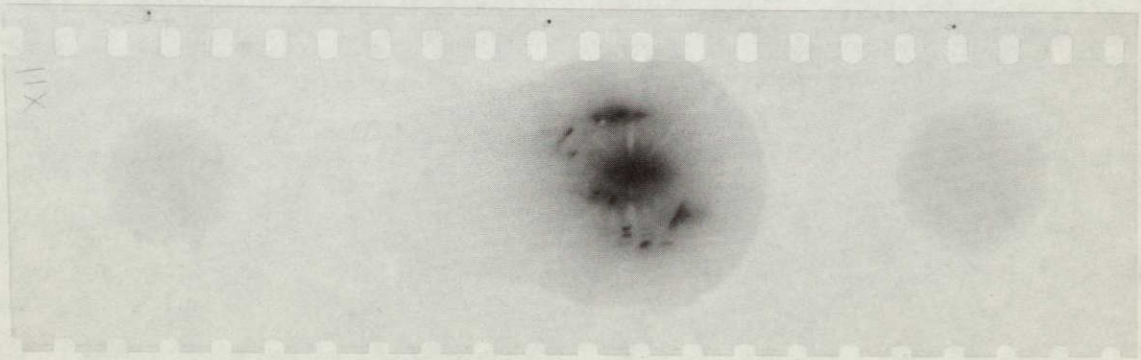

Figure 6.12 Expsoure XII June 8, 1968 (see Table III)

7.0 CONCLUSIONS

The results obtained from the March 15, 1968 flight have shown that the X-ray flux from the whole sun, during an active period close to sunspot maximum, was 1.0×10^{26} erg sec^{-1}. The active region, which had produced a small subflare a few minutes before the photographs were taken, contributed approximately 2.0×10^{25} erg sec^{-1}. The central core of the X-ray region, which we have identified with the region that produced the subflare on the basis of its correspondence to the $H\alpha$ image of the sun, was less than 30 arc-seconds wide.

The June 8, 1968 flight was successful and produced high resolution X-ray images of active regions, the solar corona and an X-ray flare.

Appendix A contains a list of the publications which have resulted from these two flights, and Appendix B contains a detailed discussion of the June 8, 1968 films as published in Science.

APPENDIX A

List of publications supported in full or in part by NASA contract/ NASW-1700:

Vaiana, G. S., Reidy, W. P., Zehnpfennig, T., VanSpeybroeck, L. P. and Giacconi, R., "X-ray Structures of the Sun During the Importance 1N Flare of 8 June 1968." 1968, Science, 161, 564.

Vaiana, G. S. and Giacconi, R., "Observation of an X-ray Flare: Spatial Distributionand Physical Parameters," Plasma Instabilities in Astrophysics; (Wentzel, D. G. and Tidman, D. A., Ed.; Gordon and Breach; 1969).

Vaiana, G. S. and Zehnpfennig, T., "Analysis of High Resolution X-ray Photographs; I: An Importance 1N Flare." 1969, Bull. Am. Astron. Soc., 1(3), 294.

Reidy, W. P. and VanSpeybroeck, L. P., "Analysis of High Resolution Solar X-ray Photographs; II: Solar Active Regions". 1969, Bull. Am. Astron. Soc., 1(3), 294.

APPENDIX B

X-ray Structures of the Sun During the Importance In Flare of 8 June 1968

Published in Science, 1968, 161, 564. Note that the "cover page photograph" and "Figure 3" referred to in this Appendix, are the same as Figures 6.6 and 6.10, respectively, of this report.

ABSTRACT

High resolution solar X-ray images were obtained with a rocket-borne grazing incidence telescope. The X-ray flare is large in extent, has fine structure and follows a neutral magnetic line. X-ray emitting coronal links interconnect active regions. The general coronal emission at the limb and several faint regions on the disc are observed.

In order to study the physical processes which govern the onset and development of solar flares, we have flown an X-ray telescope on a pointed rocket platform and obtained high resolution X-ray photographs of the sun while a flare was in progress. Structural features only a few arc seconds in extent are observed in the X-ray flare for the first time. The photographs also show X-ray emitting regions associated with plages and the general X-ray coronal emission. Spectral data were acquired by means of broad band filters; dispersed spectra of individual active regions were also obtained by means of a slitless spectrograph technique used for the first time.

X-rays from the sun are of interest both as the most sensitive indicators of solar activity and as a tool to study the physics of regions containing extremely high temperature plasmas or high energy electrons. The study of solar X-ray emission has progressed rapidly in the last few years. The progress in the field has been reviewed (1) by de Jager, Mandel'shtam, and more recently by Goldberg.

In order to define the physical parameters of interest, one needs the spatial and spectral distribution of the radiation from the regions being investigated. X-ray images of the sun using pin-hole camera techniques have been obtained by Blake, Chubb, Friedman and Unzicker (2); Russell and Pounds (3); and Zhitnik, Krutov, Malyavkin and Mandel'shtam (4). Grazing incidence telescopes of the type first suggested for use in X-ray astronomy by Giacconi and Rossi (5) have been used by Giacconi, Reidy, Zehnpfennig, Lindsay and Muney (6) and by Underwood and Muney (7). Structural details of 20 arc seconds could be resolved in the highest resolution X-ray photographs previously obtained (7). These experimenters obtained information on the spectral distribution of the radiation from particular solar regions by the use of broad band filters. On the other hand, dispersed X-ray spectra of the sun as a whole have been obtained by numerous groups (8). Our group has devoted its efforts over the last few years to the problem of simultaneously obtaining high resolution X-ray images and spectra of each individual emitting region(9).

INSTRUMENT AND EXPERIMENTAL PROGRAM

The X-ray telescope carried in this payload is of a type described previously (10) and consists of a paraboloid and hyperboloid which are co-axial and con-focal. The incident soft X-rays are reflected once from each mirror at a grazing angle and form a real image of the distant X-ray source in the focal plane. The X-ray telescope used in this experiment has a collecting area of 34 cm^2 and a focal length of 132 cm and is appreciably larger and more sensitive than any flown previously. The speed of the system is sufficiently high so that a relatively slow, high resolution film (Panatomic X) could be used even in one of the shortest exposures (2 seconds) and still yield useful film densities in the plage regions as well as in the flare. In the flight pictures, details in the flare region only 2 arc seconds in size can be distinguished.

The camera consists of a rotating 12-sided drum to which individual film and filter combinations were attached. The different filters transmit different X-ray wavelength intervals and exclude solar visible and ultraviolet radiation from the film.

A soft X-ray transmission grating was successfully used for the first time in this experiment. The grating, which was positioned immediately behind the telescope, was launched in a folded position and deployed for the last four exposures. The combination of the telescope and the grating constitutes a soft X-ray slitless spectrograph and was first suggested by Gursky and Zehnpfennig (11) and developed by Zehnpfennig (11). The grating disperses part of the radiation being focused on a given point in the focal plane into spectra of various orders which then bracket that point. The grating for this flight consisted of a 1μ thick parylene substrate upon which 1440 parallel gold strips per millimeter had been deposited by vacuum evaporation. The dispersion in the first order is 0.50 arc min/Å, or 0.15 mm/Å in the focal plane.

The experimental plan was to launch the rocket within a few minutes of the observation of a solar flare by an alarm network of ground-based solar observatories. Simultaneous ground observations were to be made in $H\alpha$, Ca K, centimeter and decameter radio, and in the 5303 Å coronal line. In addition, three experiments (12) carried on the OSO-4 satellite will be able to furnish the following: a) spectra obtained with Bragg Crystal Spectrometer on the sun as a whole (Naval Research Laboratory group), b) life history of the flare with high time resolution obtained with proportional counter technique (University of Leicester-University College of London group), and c) images of the sun obtained every 300 seconds, prior, during and after the flare with four arc minute resolution (American Science and Engineering group). When all of this information becomes available and can be correlated, we will have the most complete description of such an event yet obtained. The purpose of this note is to describe certain important qualitative features resulting from the inspection of the X-ray pictures and from the correlation with preliminary data available to us.

On June 8, 1968, the sun was moderately active. Over a dozen active regions were present on the disc, the most prominent being the one where the observed flare developed. This region (identified as McMath No. 207) had, since its first appearance on the east limb on June 2, increased in plage area and intensity, spot group area and number, 9.1 cm flux and flare activity. For a number of hours before the flare, the active region had shown brightening fluctuations. A filament associated with this region had been active in the blue wing of $H\alpha$ and underwent a "disparition brusque" some 30 minutes before the flare. Prior to disappearance the filament was located along the neutral line of the magnetic configuration, as indicated by the polarity of the spots. The observed flare was a large 1N flare of the parallel ribbon kind. It was accompanied by centimeter microwave bursts superimposed on a very small gradual rise and fall in all the microwave region of duration comparable to the $H\alpha$ flare. Continuum decameter emission began at 1600 UT and lasted through 1900 UT.

The flare was also accompanied by an ionospheric disturbance. The Hα flare onset was at about 1732 UT, reached the maximum at about 1745 UT, and lasted about 1.5 hours. The rocket was launched at 1740 UT, acquired the sun at 1742 UT and obtained exposures until 1745 UT. The pointing control, developed by the Sounding Rocket Branch of Goddard Space Flight Center, achieved the unprecedented accuracy of $\pm$ 1 second of arc jitter throughout all of the exposures.

EXPERIMENTAL RESULTS

The exposure time, filter, film and nominal wavelength pass-band for each of the exposures are listed in Table I. The analysis of the 12 exposures has just started and will require extensive data reduction. There are however a number of new experimental facts which have resulted from a "quick-look analysis" of the photographs. We believe that some of the facts have important consequences in the interpretation of solar phenomena. A few selected images (13) (or portions of images) are reproduced on the cover page and in the figures to illustrate the conclusions. The orientations of the photographs are given in the figure captions and are not the same for all cases (the cover page photograph has the same orientation as Figure 1). The most significant observations are summarized below according to the catagories a) flare, b) active regions, and c) general coronal emission.

a) Flare. The flare itself is by far the most impressive of all the X-ray emitting regions. The cover page photograph, a 6 second exposure on Pan-X film with a 3.8μ mylar filter, shows the flare somewhat over exposed in the central portion of the image. The inner structure of the flare is better displayed in Figure 2A, a 2 second exposure with a 13μ beryllium filter and Pan-X film.

We first observe that the flare region is more than an order of magnitude (13) brighter than all of the other plages, and that the X-ray emission is distributed into two main structures, each several minutes of arc long and approximately 20 seconds of arc across. One of the structures is a ribbon running from northeast to southwest; the other structure, to the south of the first, is an "S" shaped feature. We have not yet received the Hα photographs taken during our flight.

However, from correlation with a preflight $H\alpha$ image (Figure 1 and 2A'), and from discussion with P. S. McIntosh, the observer at ESSA at the time of the flare, we have been able to establish that the general structure of the X-ray flare strikingly resembles the one of $H\alpha$, and that the portions of the flare which are brighter in $H\alpha$ are also brighter in X-rays and with much higher contrast. We find that the brightest portion of the X-ray flare (part of the "S" shape structure) seems to follow the location of the active filament which had disappeared (Figure 2A and 2A'). The flare also shows many small features which are not observed in nearby active regions; for example, in the original negative of Figure 2A, two filaments about 2 seconds of arc across and separated by 5 seconds of arc are clearly visible (14).

b) Active regions. We find that all regions which are active in $H\alpha$ (Figure 1) have counterparts in the X-ray photograph (cover page); even small $H\alpha$ brightenings such as those at approximately 30° west and 70° west close to the equator have corresponding brightenings in X-rays. A closer examination reveals that the correspondence between the $H\alpha$ and X-ray images of a region depends upon the position on the solar disc. The X-ray emitting regions, when seen close to the center of the disc, seem to conform rather well with the shape and boundaries of $H\alpha$ bright regions. The X-ray images near the limb (Figure 2B) however, show a looping and interconnecting of active regions which is not found in the $H\alpha$ images (Figure 2B'); one sees X-ray structures extending 100,000 km or more above the $H\alpha$ plage. Finally, at the limb (Figure 2C and 2C') there are loops and structures similar to those seen in white light coronal photographs. The X-ray loop structure does not have a corresponding $H\alpha$ counterpart; however, spectra taken at Sacramento Peak show that the green line (5303 Å) was strong in that portion of the limb, and two days later a weak plage region rotated onto the disc.

The X-ray emitting regions appear to be the same size in the 44 Å to 60 Å and 3.5 Å to 14 Å wavelength intervals. This observation is based upon a

comparison of mylar and beryllium filter exposures which had equivalent photographic densities as a result of appropriate exposure duration ratios.

c) General corona. The general corona emission not associated with flares or plages is evident in the mylar filter exposures, such as the cover page, which include the 44 Å to 60 Å region. Since this emission does not appear in the longest exposure with the beryllium filter (3.5 Å to 14 Å), we conclude, in agreement with previous observations, that the general corona emission is somewhat softer than the plage or flare associated emission. We also find weakly emitting regions distributed over the disc which are not plage associated, and thus confirm an observation made in one of our earlier flights (10). These features are seen in the mylar filter exposure, for example in the north portion of the disc on the cover page, but cannot be found in the beryllium exposures; therefore, this emission is also softer than that associated with plages.

Finally, this flight provided the first verification of the X-ray slitless spectrograph technique. The results show that the technique is valuable where high speed is required, and it should be particularly useful in the study of transient phenomena, and in obtaining spectral data separately from each of several small active solar regions. The four transmission grating exposures contain spectra of each of the active regions including the flare. One of these exposures, Exposure X, is reproduced in Figure 3. Several emission lines or blends can be observed in the original negatives; the lines are particularly evident in the higher spectral orders. The most prominent flare line in the image (This line is also found in some of the plage spectra.) occurs at about 9.2 Å. This is consistent with either Mg XI or Fe XXI lines which have been observed by other experimenters (4, 8). The envelope of the spectra from the several regions can also be observed.

DISCUSSION AND CONCLUSIONS

Detailed comparisons with existing theories will require a quantitative analysis of this experimental data and the correlated data from other sources.

The following considerations, however, indicate certain qualitative features which must be included in models of flares and other manifestations of activity.

a) Flare. It has been shown (15) that the X-ray emission contributes a large fraction of the energy released in a flare. From the film density and the flare size, we estimate the soft X-ray output of this flare to be of the order of 10^{30} to 10^{31} ergs. We consider it important that the X-ray flare is extended in area at the time of the Hα maximum brightness. If we make the conservative assumption that the ribbons of the flare have circular cross sections with diameters equal to their observed widths, we find that the apparent volume of the flare is in excess of 10^{28} cm^3.

The spatial correspondence between the X-ray and the Hα flare indicates a close physical link between the two emission phenomena; this is puzzling because of the large difference in degree of ionization required to account for the X-ray and the Hα emissions. One possibility is to envisage spatial separation between the two regions, with a strong magnetic connection to account for the similarity in shape. The X-ray emission associated with the other plage regions suggests such a magnetic link. For the flare, however, one is faced with the difficulty of having to assume a strong stable magnetic link while at the same time requiring a sudden change of the magnetic configuration in order to account for the observed radiation.

Finally, we note the significance of the spatial association of the X-ray emission with the disappeared filament, and hence with the magnetic neutral line. A number of flare theories emphasize the role of the neutral line not only in the magnetic storage mechanism, but also in the trigger and first release process. Previously only visible light observations yielded data bearing on this question, but the X-ray emission is more directly connected to the energetic particles involved in the primary process.

b) Active regions. We interpret the X-ray images as lescriptive of the three-dimensional coronal structure of the active regions. The overriding impression one receives from the photographs is that the X-ray emitting regions resemble the Hα regions at the base of the corona, but at higher levels the X-ray emitting regions are rich in loop-like structures which interconnect Hα active regions and are largely determined by the magnetic field. This interpretation strengthens theories which attribute the extra heating in upper layers of active regions to the presence of an enhanced magnetic field. We interpret the similar size of the X-ray emitting regions in the 44 Å to 60 Å and 3.5 Å to 14 Å wavelength intervals, both at the limb and on the disc, as evidence that the X-ray active regions as a whole do not show large scale temperature structure. On the other hand, temperature structure may be present on a scale small with respect to the size of the regions, perhaps in a multilayer rope-like volume with strong magnetic field confinement.

c) General corona. By comparing the X-ray with the Hα image we associate the weakly emitting regions with the brightest portions of the chromospheric magnetic network. It has been suggested that, in the heating mechanism of the corona, the magnetic field of the network plays an important role (16). It is, therefore, tempting to link the general X-ray corona we observe at the limb to the weakly emitting regions on the disc associated with the brightest features of the network. The softness of the spectra from both regions is also consistent with our opinion that these are two views of the same type of activity.

In conclusion we realize that it will be necessary to study with comparable detail several flare events before we can determine if the features we observe are a common characteristic of all flares. The overriding impression we obtain from the analysis of these photographs is that more detailed understanding of solar phenomenology can be achieved by modest improvement of spatial resolution in the X-ray region of the spectra. The dominant role played

by magnetic fields in the storage and release of energy in the solar atmosphere can be perceived from the correlation between $H\alpha$ and X-ray structures, the existence of loops interconnecting active regions, and the development of the X-ray flare along a neutral magnetic field line.

G. S. Vaiana
W. P. Reidy
T. Zehnpfennig
L. VanSpeybroeck
R. Giacconi
American Science & Engineering
Cambridge, Massachusetts
July 9, 1968

References and Notes

1 C. de Jager, Ann. Ap. 28, 125 (1965); S. L. Mandel'shtam, Space Sci. Rev. 4, 587 (1965); L Goldberg, Ann. Rev. Astron. Ap. 5, 279 (1967).

2. R. L. Blake, T. A. Chubb, H. Friedman, and A. E. Unzicker, Astrophys. J. 142, 1 (1965).

3. P. C. Russell, Nature 205, 684 (1965); K. A. Pounds and P. C. Russell, Space Research, 6, 32 (1966).

4. I. A. Zhitnik, V. V. Krutov, L. P. Malyavkin and S. L. Mandel'shtam, Space Research, 7, 1263 (1967)

5. R. Giacconi and B. B. Rossi, J. Geophys. Res. 65, 773 (1960).

6. R. Giacconi, W. P. Reidy, T. Zehnpfennig, J. C. Lindsay, W. S. Muney, Astrophys. J. 142, 1274 (1965).

7. J. H. Underwood and W. S. Muney, Solar Physics 1, 129 (1967).

8. H. R. Rugge and A. B. C. Walker, Space Research 8, (1967); G. Fritz, R. W Kreplin, J. F. Meekins, A. E. Unzicker and H. Friedman, Astrophys. J. 148, L133 (1967); W. M. Neupert, W. Gates, M. Swartz, and R. Young, Astrophys. J. 149, L79 (1967); K. Evans and K. A. Pounds, Astrophys. J. 152, 319 (1968).

9. This effort is being conducted under the sponsorship of the Solar Physics Branch of NASA Headquarters. The payload used in this experiment is a scaled-down version of a more sophisticated experiment we are preparing for flight in a manned solar mission (Apollo Telescope Mount). This mission, which is being carried out by NASA's Marshall Space Flight Center. will allow almost continued observations for a full solar rotation.

10. W. P. Reidy, G. S. Vaiana, T. Zehnpfennig, R. Giacconi, Astrophys. J. 151, 333 (1968).

11. H. Gursky and T. Zehnpfennig, Appl. Optics 5, 875 (1966); T. Zehnpfennig, Appl. Optics 5, 1855 (1966).

12. Papers on the performance of and on the preliminary result from the three instruments have been presented at the AAS Special Meeting on Solar Astronomy, Tucson, Arizona, (February 1-3, 1968) by H. Friedman et al.; J. L. Culhane et al.; F. R. Paolini et al.; and at the Midwest Cosmic Ray Conference, Iowa City, Iowa (March 1-2, 1968) by F. R. Paolini et al. and G. S. Vaiana et al.

13. The 10^3 dynamic range of the negatives is larger than that of the printing paper, and we have had to compress the original density of the negatives in order to show both the brightest and faintest features; this has resulted in a considerable loss of contrast in the print. The faint halo visible around very intense features is an instrumental effect due to the wings of the telescope response to a point source. The dark rays in the halo are shadows of the ribs in the telescope aperture plates.

14. The observation of such fine details is only possible near the optical axis where the best telescope resolution is obtained; there are, however, active regions which are as close to the optical axis as the flare and do not show the same type of fine features.

15. A Bruzek, Solar Physics Xanthakis, Ed. (Interscience Publishers, London and New York 1967) p. 414.

16. D. E. Osterbrock, Astrophys. J. 134, 347, 1961.

17. We thank the staffs of ESSA; Sacramento Peak; McMath; Lockheed and Sagamore Hill Observatories for their support in providing flare alarm

and ground measurements. In particular we thank D. Bucknam and R. Decker (ESSA) for their excellent coordination of the alarm network. We are indebted to R. Howard and H. Zirin (Mount Wilson and Palomar Observatories); W. Livingston and N. Sheely (Kitt Peak Observatory); W. Curtis (High Altitude Observatory) for additional ground measurements. We acknowledge the help of P. S. McIntosh in interpreting the Hα features discussed in the text. We also thank the personnel both of the Sounding Rocket Branch of Goddard Space Flight Center and of the White Sands Missile Range who supported us without complaint during the many days we waited for the flare. Finally, we thank A. De Caprio, R. Haggerty, H. Manko and D. Yansen (AS&E) for their valuable technical support.

18. This work was performed under contracts NASW-1555, NASW-1700 and NAS 5-9041.

TABLE I

Films, Filters and Exposure Times

Frame	Exposure Time	Filter[1]	Film[3]
I	22 seconds	13μ beryllium	103-0 un-TC
II	2 seconds	50μ beryllium	Pan X TC
III	6 seconds	13μ beryllium	Pan X TC
IV	19 seconds	13μ beryllium	Pan X un-TC
V	2 seconds	13μ beryllium	Pan X TC
VI	6 seconds	3.8μ mylar[2]	Pan X un-TC
VII	18 seconds	2.5μ steel	103-0 un-TC
VIII	2 seconds	visible	Pan X TC
IX	6 seconds	3.8μ mylar[2]	Ilford Special[4]
X	6 seconds	13μ beryllium	103-0 un-TC[4]
XI	22 seconds	13μ beryllium	103-0 un-TC[4]
XII	52 seconds	13μ beryllium	103-0 un-TC[4]

(1) The filter thicknesses given are nominal. The approximate wavelength pass-bands are: 13μ beryllium (3.5 Å to 14 Å); 50μ beryllium (3.5 Å to 10 Å); and 3.8μ mylar (3.5 Å to 14 Å and 44 Å to 60 Å).

(2) About 2200 Å of aluminum was evaporated on the mylar.

(3) "TC" or "un-TC" are with or without a protective gelatin layer, respectively.

(4) Exposures with the transmission grating

NOT REPRODUCIBLE

DZ-073

Figure 1. A photograph of the sun in Hα light at 1555 UT, approximately two hours before the X-ray observations. There is a striking correlation between the Hα active regions and the X-ray emitting regions shown on the cover page. On this photograph and the cover, heliocentric north is approximately 30° counterclockwise from the bottom and east is on the right. (By courtesy of the ESSA Boulder Observatory)

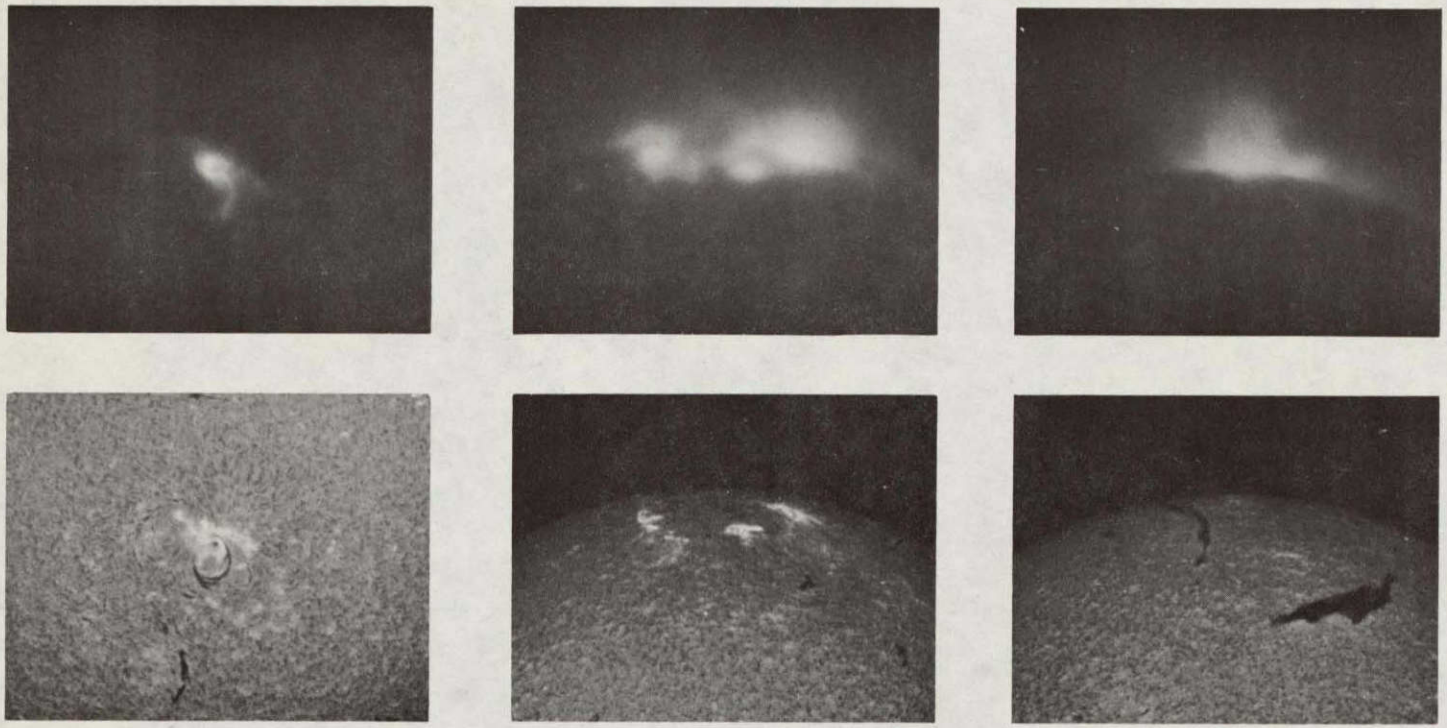

DZ-072

Figure 2. Figures 2A, 2B, and 2C are X-ray images of selected portions of the sun; Figures 2A', 2B', and 2C' are $H\alpha$ photographs of the corresponding portions taken two hours prior to the flight. Corresponding images are orientated the same way. Figure 2A is the flare region in 3.5 Å to 14 Å pass band (Exposure V). The "S" shaped structure (brightest portion of the flare) follows the neutral line marked by the filament (Figure 2A'), which later disappeared, as discussed in the text. Portions of the filament extend to the top and left of the sunspot and then up. Figure 2B shows the group of plages in the southwest quadrant close to the limb. At least three arches interconnecting regions can be distinguished. Notice the absence of the connections in $H\alpha$. Figure 2C is the loop structure at the southeast. It extends over 150,000 km above the limb; no counterpart of the loop is visible in $H\alpha$ but the green coronal line (5303 Å) was strong in that portion of the limb, and a plage region rotated from the limb two days later. (The $H\alpha$ photographs by courtesy of ESSA Boulder Observatory)